

# A new measure for cosmic shear

Peter Schneider, Ludovic van Waerbeke, Bhuvnesh Jain & Guido Kruse

Max-Planck-Institut für Astrophysik  
Postfach 1523  
D-85740 Garching, Germany

## Abstract

Cosmic shear, i.e., the distortion of images of high-redshift galaxies through the tidal gravitational field of the large-scale matter distribution in the Universe, offers the opportunity to measure the power spectrum of the cosmic density fluctuations without any reference to the relation of dark matter to luminous tracers. We consider here a new statistical measure for cosmic shear, the aperture mass  $M_{\text{ap}}(\theta)$ , which is defined as a spatially filtered projected density field and which can be measured directly from the image distortions of high-redshift galaxies. By selecting an appropriate spatial filter function, the dispersion of the aperture mass is a convolution of the power spectrum of the projected density field with a narrow kernel, so that  $\langle M_{\text{ap}}(\theta) \rangle$  provides a well localized estimate of the power spectrum at wavenumbers  $s \sim 5/\theta$ . We calculate  $\langle M_{\text{ap}}^2 \rangle$  for various cosmological models, using the fully non-linear power spectrum of the cosmic density fluctuations. The non-linear evolution yields a significant increase of  $\langle M_{\text{ap}}^2 \rangle$  relative to the linear growth on scales below  $\sim 1/2$  degree.

The third-order moment of  $M_{\text{ap}}$  can be used to define a skewness, which is a measure of the non-Gaussianity of the density field. We present the first calculation of the skewness of the shear in the frame of quasi-linear theory of structure growth. We show that it yields a sensitive measure of the cosmological model; in particular, it is independent of the normalization of the power spectrum.

Several practical estimates for  $\langle M_{\text{ap}}^2 \rangle$  are constructed and their dispersions calculated. On scales below a few arcminutes, the intrinsic ellipticity distribution of galaxies is the dominant source of noise, whereas on larger scales, the cosmic variance becomes the most important contribution. We show that measurements of  $M_{\text{ap}}$  in two adjacent apertures are virtually uncorrelated, which implies that an image with side-length  $L$  can yield  $[L/(2\theta)]^2$  mutually independent estimates for  $M_{\text{ap}}$ . We show that one square degree of a high-quality image is sufficient to detect the cosmic shear with the  $M_{\text{ap}}$ -statistics on scales below  $\sim 10$  arcmin, and to estimate its amplitude with an accuracy of  $\sim 30\%$  on scales below  $\sim 5$  arcmin.

# 1 Introduction

Gravitational light deflection caused by an inhomogeneous distribution of matter in the Universe causes observable effects on the images of distant sources. Whereas mass concentrations on scales of galaxies and clusters yield strong lensing effects – multiple images, (radio) rings, and giant luminous arcs – density inhomogeneities on larger scales or with less concentration causes weak lensing effects. In particular, the shape and observable flux of distant galaxies is affected by the tidal component of the gravitational field and the density fluctuations along their lines-of-sight, respectively. Whereas these lensing effects are too weak to be detected in individual galaxy images, they can be investigated statistically. Assuming that the intrinsic orientations of galaxies are random, cosmic shear – i.e., the line-of-sight integrated tidal gravitational field – can be detected as a net alignment of galaxy images on a given patch of the sky.

The statistical properties of the cosmic shear are directly linked to the statistical properties of the density inhomogeneities (Gunn 1967, Blandford & Jaroszyński 1981). In particular, any two-point statistics, like the two-point correlation function of galaxy image ellipticities or the mean quadratic image ellipticity, can be expressed as a redshift integral over the power spectrum of the cosmological density fluctuations, weighted by geometrical factors depending on the source redshift distribution (Blandford et al. 1991; Miralda-Escudé 1991; Kaiser 1992, 1996, hereafter K96; Villumsen 1996). These geometrical factors, as well as the redshift evolution of the power spectrum, depend on the cosmological model. Therefore, a quantitative analysis of the cosmic shear statistics can provide strong constraints on cosmological parameters and the shape of the fluctuation power spectrum.

It should be stressed that this approach to determine the density fluctuations in the Universe does not rely on assumptions about the relation between luminous and dark matter. It is therefore of comparable interest as the investigation of the cosmic microwave background radiation. In fact, these two approaches are complementary: Whereas the CMB measures the fluctuation spectrum at the time of recombination, where the density perturbations were small, the cosmic shear probes the fluctuation spectrum at relatively small redshifts,  $z \sim 0.5$ , where it has become non-linear on scales smaller than  $\sim 5$  Mpc. Secondly, due to the finite thickness of the recombination shell, the CMB is expected to show no structure on angular scales below  $\sim 5$  arcmin, corresponding to comoving scales of  $\sim 10$  Mpc, whereas cosmic shear can probe the density fluctuations also on much smaller scales. Finally, a comparison of the results from both techniques can provide a beautiful confirmation of the gravitational instability theory of structure growth.

The above-mentioned authors have calculated the two-point correlation function of galaxy image ellipticities and the rms image ellipticity using the linear theory of density instabilities. On angular scales below  $\sim 20$  arcmin, one starts to probe the density fluctuation spectrum on scales below  $\sim 5h^{-1}$  Mpc (where  $h$  is the current value of the Hubble constant in units of 100 km/s/Mpc) where the density fluctuations are nonlinear. Jain & Seljak (1997; hereafter JS) generalized the previous investigations of cosmic shear to the fully non-linear evolution of the power spectrum, and found that the expected rms shear increases by about a factor of two on small scales, relative to the predictions from the linear evolution of the power spectrum. Given that the expected rms shear on arcminutes scale is of the order of a few percent, this enhancement dramatically increases the possibility to detect cosmic shear with currently existing instruments and

data analysis techniques. In fact, deep observations of fields around radio QSOs have revealed the presence of a coherent shear pattern (Fort et al. 1996, Bower & Smail 1997) which has been interpreted as cosmic shear (Schneider et al. 1997), though the selection of these fields was based on the magnification bias hypothesis (Bartelmann & Schneider 1994, Benítez & Martínez-González 1997, and references therein) for these luminous radio QSOs. Therefore, these measurements should not be interpreted in any statistical sense; nonetheless, they have shown that a shear of a few percent is measurable even on scales as small as 2 arcmins.

An attempt to measure cosmic shear on a single  $\sim 9$  arcmin field did not yield a significant signal (Mould et al. 1994), though a reanalysis of the same data with a somewhat less conservative approach found a fairly high significance (Villumsen 1995). The development of wide-field cameras and sophisticated data analysis methods specifically targeted at weak lensing studies (Bonnet & Mellier 1995; Kaiser, Squires & Broadhurst 1995; Luppino & Kaiser 1996; van Waerbeke et al. 1997) suggest that the discovery of cosmic shear in random fields, and its quantitative analysis, are just lurking around the corner.

Higher-order than two-point statistics for cosmic shear are difficult to estimate analytically. Bernardeau, van Waerbeke & Mellier (1997; hereafter BvWM) have calculated the skewness of the projected surface mass density field, using the quasi-linear theory of structure growth. They pointed out that the skewness is a powerful indicator for the cosmic density parameter; in particular, it is independent of the normalization of the power spectrum, and fairly independent of the cosmological constant. A practical difficulty related to that measure is that the projected surface mass density is less directly linked with observables. Whereas it is tightly related to the magnification of sources, this by itself is difficult to observe. One would therefore like to measure the skewness of a quantity that is directly related to the shear, which is observable from image ellipticities.

Such a quantity is provided by the  $M_{\text{ap}}$ -statistics, introduced by Kaiser et al. (1994) and Schneider (1996), as a generalization of the  $\zeta$ -statistics introduced by Kaiser (1995). The latter yields an unbiased estimate of the mean surface mass density within a circle, minus the mean surface mass density within an annulus surrounding this circle, and can be obtained from the shear within the annulus. First applied to the cluster MS1224 (Fahlman et al. 1994), this “aperture densitometry” has yielded a lower bound on the mass-to-light ratio in the center of this cluster which is considerably larger than values typically found in clusters by other means.

The  $M_{\text{ap}}$ -statistics, which measures the projected density field filtered with a compensated filter function, combines the properties that it is directly related to the projected mass density, and that it is obtainable from the shear, i.e., observable through image ellipticities. Furthermore, in contrast to the mean shear within a circle, which is a two-component quantity from which no non-trivial third-order moment can be defined, the  $M_{\text{ap}}$ -statistics is a scalar whose skewness is well-defined. Schneider (1996) has suggested that the  $M_{\text{ap}}$ -statistics can be used to search for (dark) matter concentrations on high-quality wide-field images.

In this paper we shall investigate the  $M_{\text{ap}}$ -statistics as a measure for cosmic shear. In Sect. 2 we briefly review the basic equations for the light propagation in an inhomogeneous Universe, thereby introducing our notation. The two-point  $M_{\text{ap}}$ -statistics is introduced in Sect. 3. It is shown that the dispersion of  $M_{\text{ap}}$  on a certain angular scale can be expressed as an integral over the power spectrum of the projected surface mass density,

times a filter function containing this scale. This filter function is shown to be quite narrow, so that  $\langle M_{\text{ap}}^2(\theta) \rangle$  provides a fairly localized estimate of the power spectrum. This is contrasted with the rms shear averaged on circles, for which the corresponding filter function is very broad.

For various cosmological models, the dispersion of  $\langle M_{\text{ap}}^2 \rangle$  is calculated, for both the linear and fully non-linear growth of density perturbations, and compared to the rms mean shear. In Sect. 4, we calculate the skewness of  $M_{\text{ap}}$ , following closely the treatment of BvWM, i.e., applying the quasi-linear theory of structure growth. Sect. 5 is devoted to practical estimators of  $\langle M_{\text{ap}}^2 \rangle$  and the skewness, and their respective accuracies. A practical advantage of the  $M_{\text{ap}}$ -statistics over the rms shear is that values of  $M_{\text{ap}}$  measured in neighboring apertures are virtually independent, whereas the mean shear inside a circle has a very large correlation length. This fact is of particular relevance for measurements of cosmic shear on small angular scales, using wide-field cameras. For a fixed total solid angle of available data, the signal-to-noise ratio for the measurement of  $\langle M_{\text{ap}}^2 \rangle$  is obtained for  $\theta \sim 2'$ , somewhat dependent on the kurtosis of the density field. Depending on cosmology, a measurement of the dispersion of  $M_{\text{ap}}$  with an accuracy of  $\sim 20\%$  should be possible from one square-degree of deep imaging data. We discuss our results in Sect. 6. In the Appendix, we consider several approximations which are used throughout the main body of the paper. We focus on the contributions to the skewness which arise even in the case of Gaussian density fluctuations, and find that by including these effects, the skewness changes by  $\sim 10\%$ , which justifies the use of our approximations.

## 2 Light propagation in slightly inhomogeneous Universes

We shall use a notation similar to K96 and JS. The metric of the homogeneous Universe is written in the form

$$ds^2 = c^2 dt^2 - a^2(t) [dw^2 + f_K^2(w)d\omega^2] , \quad (2.1)$$

where  $a(t) = (1 + z)^{-1}$  is the dimensionless cosmic scale factor, normalized to unity today;  $w$  is a radial coordinate, and  $f_K(w)$  is the *comoving angular diameter distance* to distance  $w$ . The spatial curvature

$$K = \left( \frac{H_0}{c} \right)^2 (\Omega_d + \Omega_v - 1) , \quad (2.2)$$

is related to the present day value of the density parameters  $\Omega_d$  and  $\Omega_v$  in dust and in vacuum energy, in terms of which  $f_K(w)$  reads

$$f_K(w) = \begin{cases} K^{-1/2} \sin(\sqrt{K}w) & \text{for } K > 0 , \\ w & \text{for } K = 0 , \\ (-K)^{-1/2} \sinh(\sqrt{-K}w) & \text{for } K < 0 . \end{cases} \quad (2.3)$$

The angular diameter distance  $D(z_1, z_2)$  is conveniently expressed in terms of  $f_K$  by

$$D(z_1, z_2) = \frac{1}{1 + z_2} f_K(w_2 - w_1) , \quad (2.4)$$

$z_1 \leq z_2$ , where the  $w_i$  are the radial distances corresponding to redshifts  $z_i$ ,

$$w = \int_0^z dz' \frac{c}{H} = \frac{c}{H_0} \int_0^z \frac{dz'}{\sqrt{(1+z')^3 \Omega_d + (1+z')^2 (1 - \Omega_d - \Omega_v) + \Omega_v}} . \quad (2.5)$$

Light propagation in a weakly inhomogeneous Universe has been investigated in many papers (e.g., Blandford et al. 1991; Seitz, Schneider & Ehlers 1994, and references therein). We shall use the results of these papers in the following form:

Consider a bundle of light rays intersecting at the observer. Each of these rays is characterized by the angle  $\boldsymbol{\theta}$  it encloses with a fiducial ray. Let  $\mathbf{x}(\boldsymbol{\theta}, w)$  denote the comoving transverse separation of the ray characterized by  $\boldsymbol{\theta}$  from the fiducial ray; it satisfies the propagation equation

$$\frac{d^2 \mathbf{x}}{dw^2} + K \mathbf{x} = -\frac{2}{c^2} \left[ \nabla_{\perp} \Phi(\mathbf{x}(\boldsymbol{\theta}, w), w) - \nabla_{\perp} \Phi^{(0)}(w) \right] , \quad (2.6)$$

where  $\Phi(\mathbf{x}(\boldsymbol{\theta}, w), w)$  is the Newtonian gravitational potential at comoving distance  $w$  and comoving perpendicular separation  $\mathbf{x}(\boldsymbol{\theta}, w)$  from the fiducial ray,  $\Phi^{(0)}(w)$  is the potential along the fiducial ray, and  $\nabla_{\perp} = \left( \frac{\partial}{\partial x_1}, \frac{\partial}{\partial x_2} \right)$  is the transverse gradient operator *in comoving coordinates*. Here we have assumed that the fiducial ray propagates nearly parallel to the local  $x_3$ -direction, and since all angles involved are small, all rays considered propagate nearly parallel to this direction. If the Newtonian potential vanishes,  $\mathbf{x}(\boldsymbol{\theta}, w) = f_K(w) \boldsymbol{\theta}$ , in agreement with the identification of  $f_K(w)$  as comoving angular diameter distance. A formal solution to (2.6) is obtained from the Greens function of the operator on the left-hand side of (2.6), yielding

$$\mathbf{x}(\boldsymbol{\theta}, w) = f_K(w) \boldsymbol{\theta} - \frac{2}{c^2} \int_0^w dw' f_K(w-w') \left[ \nabla_{\perp} \Phi(\mathbf{x}(\boldsymbol{\theta}, w'), w') - \nabla_{\perp} \Phi^{(0)}(w') \right] . \quad (2.7)$$

A source at  $w$  with comoving distance  $\mathbf{x}$  from the fiducial ray will be seen in the absence of light deflection at an angle  $\boldsymbol{\beta} = \mathbf{x}/f_K(w)$ , which we shall call the unlensed source position. Defining, as in usual lens theory, the Jacobian matrix  $\mathcal{A}$  as

$$\mathcal{A}(\boldsymbol{\theta}, w) = \frac{\partial \boldsymbol{\beta}}{\partial \boldsymbol{\theta}} = \frac{1}{f_K(w)} \frac{\partial \mathbf{x}}{\partial \boldsymbol{\theta}} , \quad (2.8)$$

we obtain from differentiation of (2.7),

$$\mathcal{A}_{ij}(\boldsymbol{\theta}, w) = \delta_{ij} - \frac{2}{c^2} \int_0^w dw' \frac{f_K(w-w') f_K(w')}{f_K(w)} \Phi_{,ik}(\mathbf{x}(\boldsymbol{\theta}, w'), w') \mathcal{A}_{kj}(\boldsymbol{\theta}, w') , \quad (2.9)$$

where indices  $i$  on  $\Phi$  preceded by a comma denote partial derivatives w.r.t.  $x_i$ . In general this is not an explicit equation for  $\mathcal{A}$ , since in order to calculate  $\mathcal{A}$ , one first has to solve for the ray position  $\mathbf{x}(\boldsymbol{\theta}, w)$  and then solve the integral equation (2.9) for  $\mathcal{A}$ . However, for weak gravitational fields which are of interest to us here, one can expand  $\mathcal{A}$  in powers of the Newtonian potential  $\Phi$ , and keep only the lowest order term; this results in

$$\mathcal{A}_{ij}(\boldsymbol{\theta}, w) = \delta_{ij} - \frac{2}{c^2} \int_0^w dw' \frac{f_K(w-w') f_K(w')}{f_K(w)} \Phi_{,ij}(f_K(w') \boldsymbol{\theta}, w') . \quad (2.10)$$

Hence, to linear order in  $\Phi$ , the distortion is obtained by integrating the second derivatives of the potential along the unperturbed ray. This feature allows for a dramatic simplification of the calculations below. In the Appendix, we shall consider some higher-order

terms for  $\mathcal{A}$  corresponding to lens-lens coupling and to dropping the ‘Born approximation’; i.e., we shall calculate  $\mathcal{A}$  up to second order in  $\Phi$ . Also note that  $\mathcal{A}$  given in (2.10) is symmetric. One can therefore define a deflection potential,

$$\psi(\boldsymbol{\theta}, w) = \frac{2}{c^2} \int_0^w dw' \frac{f_K(w-w')}{f_K(w') f_K(w)} \Phi(f_K(w')\boldsymbol{\theta}, w'), \quad (2.11)$$

in terms of which one can treat lensing by large-scale structures similarly to the single lens-plane case; e.g., the corresponding ‘surface mass density’  $\kappa(\boldsymbol{\theta}, w)$  and shear  $\gamma(\boldsymbol{\theta}) = \gamma_1 + i\gamma_2$  are given as

$$\begin{aligned} \kappa(\boldsymbol{\theta}, w) &= \frac{1}{2} (\psi_{,11} + \psi_{,22}) , \\ \gamma(\boldsymbol{\theta}, w) &= \frac{1}{2} (\psi_{,11} - \psi_{,22}) + i\psi_{,12} , \end{aligned} \quad (2.12)$$

where indices on  $\psi$  separated by a comma denote partial derivatives with respect to  $\theta_i$ . In particular,  $\mathcal{A}_{ij} = \delta_{ij} - \psi_{,ij}$ . Thus, one can consider the surface mass density  $\kappa$  – or its associated deflection potential  $\psi$  – as the fundamental quantity, and in fact it is the only quantity which is probed by cosmic shear measurements. One obtains from (2.11) and (2.12), by adding a term  $\Phi_{,33}$  to the integrand which cancels out upon  $w$ -integration, and by using Poisson’s equation in the form

$$\nabla^2 \Phi = \frac{3H_0^2 \Omega_d}{2a} \delta , \quad (2.13)$$

the following expression for the projected density field:

$$\kappa(\boldsymbol{\theta}, w) = \frac{3}{2} \left( \frac{H_0}{c} \right)^2 \Omega_d \int_0^w dw' \frac{f_K(w-w') f_K(w')}{f_K(w)} \frac{\delta(f_K(w')\boldsymbol{\theta}, w')}{a(w')} , \quad (2.14)$$

where  $\delta(\mathbf{x}, w)$  is the density contrast. The projected density field depends on the source redshift (or distance). We shall assume that one observes the shear through a population of galaxies for which only the redshift probability distribution  $p_z(z)$  is known, or equivalently,  $p_w(w)dw = p_z(z)dz$ . Then, the source distance-averaged projected mass density becomes

$$\kappa(\boldsymbol{\theta}) := \int dw p_w(w) \kappa(\boldsymbol{\theta}, w) = \frac{3}{2} \left( \frac{H_0}{c} \right)^2 \Omega_d \int_0^{w_H} dw g(w) f_K(w) \frac{\delta(f_K(w)\boldsymbol{\theta}, w)}{a(w)} , \quad (2.15)$$

where

$$g(w) := \int_w^{w_H} dw' p_w(w') \frac{f_K(w'-w)}{f_K(w')} \quad (2.16)$$

is the source-averaged distance ratio  $D_{\text{ds}}/D_s$  for a density fluctuation at distance  $w$ , and  $w_H$  is the comoving distance to the horizon, obtained by putting  $z = \infty$  in (2.5). In this paper, we shall consider two different redshift distributions of sources. In the first case, all sources are assumed to reside at the same redshift  $z_s$ , so that

$$p_z(z) = \delta_D(z - z_s) . \quad (2.17)$$

More realistically, we consider a redshift distribution of the form (e.g., Smail et al. 1995)

$$p_z(z) \propto z^2 \exp(-[z/z_0]^\beta) . \quad (2.18)$$

The mean redshift of this distribution is proportional to  $z_0$  and depends on the parameter  $\beta$  which describes how quickly the distribution falls off towards higher redshifts. In particular, for  $\beta = 1.5$  (a value that we shall use throughout),  $\langle z \rangle = 1.505z_0$ .

### 3 Two-point $M_{\text{ap}}$ -statistics

#### 3.1 The power spectrum of the projected density field

Provided the density contrast  $\delta$  is a homogeneous and isotropic random field, so is the projected density  $\kappa$ . Consider the Fourier transform of the projected density field,

$$\tilde{\kappa}(\mathbf{s}) := \int d^2\theta \kappa(\boldsymbol{\theta}) e^{-i\boldsymbol{\theta}\cdot\mathbf{s}} . \quad (3.1)$$

We define the power spectrum  $P_\kappa(s)$  of  $\kappa$  by

$$\langle \tilde{\kappa}(\mathbf{s}) \tilde{\kappa}^*(\mathbf{s}') \rangle = (2\pi)^2 \delta_{\text{D}}(\mathbf{s} - \mathbf{s}') P_\kappa(|\mathbf{s}|) , \quad (3.2)$$

where the Dirac delta ‘function’  $\delta_{\text{D}}$  occurs because  $\kappa(\boldsymbol{\theta})$  is a homogeneous random field, and the dependence of  $P_\kappa$  on the modulus of  $\mathbf{s}$  only expresses the fact that  $\kappa$  is an isotropic random field. Following K96, we can calculate  $P_\kappa(s)$  from the power spectrum of the density fluctuations, defined accordingly by

$$\langle \tilde{\delta}(\vec{k}) \tilde{\delta}^*(\vec{k}') \rangle = (2\pi)^3 \delta_{\text{D}}(\vec{k} - \vec{k}') P(|\vec{k}|) . \quad (3.3)$$

The derivation of the Fourier-space analog of Limber’s equation in K96 is valid provided the power spectrum  $P$  does not evolve appreciably on timescales corresponding to the light travel time across the largest significant fluctuations, and provided the typical source distance is much larger than the largest-scale fluctuations. With these two assumptions, K96 (see also Kaiser 1992) obtains

$$P_\kappa(s) = \frac{9}{4} \left( \frac{H_0}{c} \right)^4 \Omega_{\text{d}}^2 \int_0^{w_{\text{H}}} dw \frac{g^2(w)}{a^2(w)} P\left(\frac{s}{f_K(w)}; w\right) . \quad (3.4)$$

The second argument of  $P$  indicates that the power spectrum evolves (slowly) with redshift. We shall later derive an analogous relation for the three-point function, using the same strategy as in the derivation of (3.4). Since  $s$  is the Fourier-conjugate of the angle  $\theta$ , we can relate an angular scale to its corresponding  $s$  by  $s = 2\pi/\theta = 2.16 \times 10^4 (\theta/1 \text{ arcmin})^{-1}$ .

In Fig. 1, we have plotted  $P_\kappa(s)$  for five different cosmological models. For three of them, the power spectrum  $P(k)$  is approximately cluster normalized, which corresponds to  $\sigma_8 \approx 0.6$  for an Einstein-de Sitter universe (EdS,  $\Omega_{\text{d}} = 1$ ,  $\Omega_{\text{v}} = 0$ ),  $\sigma_8 = 1$  for both an open universe (OCDM,  $\Omega_{\text{d}} = 0.3$ ,  $\Omega_{\text{v}} = 0$ ) and a spatially flat universe with cosmological constant ( $\Lambda$ CDM,  $\Omega_{\text{d}} = 0.3$ ,  $\Omega_{\text{v}} = 0.7$ ). In all these cases, we have used the CDM spectrum as given by Bardeen et al. (1986), but set the shape parameter of

the linear power spectrum to  $\Gamma = 0.25$ , which yields the best fit to the observed two-point correlation function of galaxies (Efstathiou 1996). The remaining two cosmological models have EdS geometry, but either a higher normalization ( $\sigma_8 = 1$ , approximately corresponding to the COBE normalization) or a different shape parameter ( $\Gamma = 0.5$ , corresponding to the original definition for  $\Gamma$  if  $H_0 = 50 \text{ km/s/Mpc}$ ). For each model, the projected power spectrum has been calculated for a linearly-evolved cosmological power-spectrum (thin curves), and for the fully non-linear power spectrum, following the prescriptions of Hamilton et al. (1991), Jain, Mo & White (1995), and Peacock & Dodds (1996) – we used the fit formulae of the latter paper throughout.

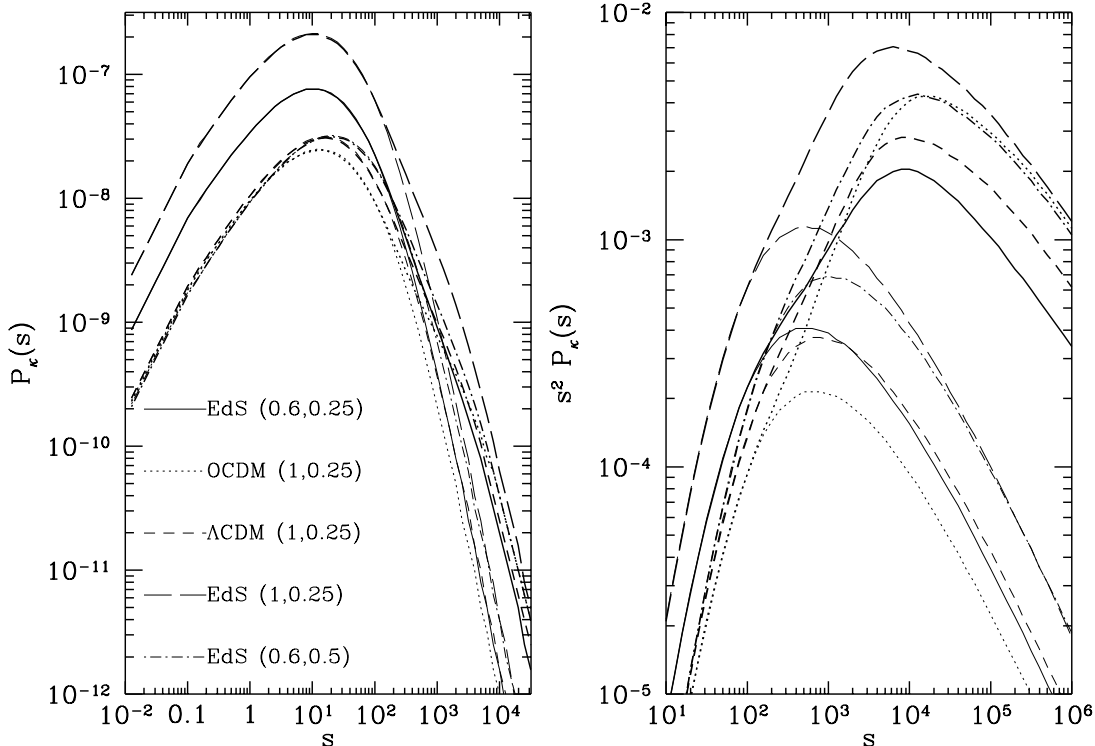


**Fig. 1.** The power spectrum  $P_\kappa(s)$  of the projected density field, as defined in (3.4), for five different cosmological models, as indicated by the line types; the numbers in parenthesis are  $(\sigma_8, \Gamma)$ . For each cosmological model, the thin curves correspond to the linear evolution of the power spectrum  $P(k, a)$ , whereas the thick curves are calculated with the fully non-linear evolution of the power spectrum, as given in Peacock & Dodds (1996). For this plot, the redshift distribution (2.18) was used, with  $z_0 = 1$  and  $\beta = 1.5$ . Note that the large amplitude of the EdS model with  $\gamma = 0.25$  relative to the OCDM and  $\Lambda$ CDM model is due to the factor  $\Omega_d^2$  in (3.4)

### 3.2 The $M_{\text{ap}}$ -statistics

Define the aperture mass by

$$M_{\text{ap}}(\theta) := \int d^2\vartheta U(|\vartheta|) \kappa(\vartheta), \quad (3.5)$$

where the integral extends over a circle of angular radius  $\theta$ , and  $U(\vartheta)$  is a continuous weight function which vanishes for  $\vartheta > \theta$ . Provided  $U$  is a compensated filter function, i.e.,



$$\int_0^\theta d\vartheta \vartheta U(\vartheta) = 0, \quad (3.6)$$

one can express  $M_{\text{ap}}$  in terms of the tangential component  $\gamma_t$  of the shear inside the circle (Kaiser et al. 1994; Schneider 1996),

$$M_{\text{ap}}(\theta) = \int d^2\vartheta Q(|\vartheta|) \gamma_t(\vartheta), \quad (3.7)$$

where

$$Q(\vartheta) = \frac{2}{\vartheta^2} \int_0^\vartheta d\vartheta' \vartheta' U(\vartheta') - U(\vartheta), \quad (3.8)$$

and the tangential component of the shear at a position  $\vartheta = (\vartheta \cos \varphi, \vartheta \sin \varphi)$  is

$$\gamma_t(\vartheta) = -\mathcal{R}e(\gamma(\vartheta) e^{-2i\varphi}). \quad (3.9)$$

The useful property of  $M_{\text{ap}}$  is thus that, on the one hand, it yields a spatially filtered version of the projected density field, and on the other hand, that it can be expressed simply in terms of the shear. Since in the weak lensing regime, the observed galaxy ellipticities provide an unbiased estimate of the local shear,  $M_{\text{ap}}$  is directly related to observables.

Obviously, the ensemble average of  $M_{\text{ap}}$  vanishes,  $\langle M_{\text{ap}} \rangle = 0$ . The dispersion of  $M_{\text{ap}}$  can be calculated as follows:

$$\begin{aligned} \langle M_{\text{ap}}^2(\theta) \rangle &= \int d^2\theta' U(\theta') \int d^2\vartheta U(\vartheta) \langle \kappa(\theta') \kappa(\vartheta) \rangle \\ &= \int d^2\theta' U(\theta') \int d^2\vartheta U(\vartheta) \int \frac{d^2s}{(2\pi)^2} e^{i\mathbf{s} \cdot (\theta' - \vartheta)} P_\kappa(s) \\ &= 2\pi \int_0^\infty ds s P_\kappa(s) \left( \int_0^\theta d\vartheta \vartheta U(\vartheta) J_0(s\vartheta) \right)^2, \end{aligned} \quad (3.10)$$

where we used in the first step that the two-point correlation function is the Fourier transform of the power spectrum, and the Bessel function  $J_0$  comes from the angular integrations in  $\theta'$  and  $\vartheta$ .

The choice of the weight function  $U(\vartheta)$  is arbitrary at this point. We shall write  $U(\vartheta) = u(\vartheta/\theta)/\theta^2$ , with  $u(x) = 0$  for  $x > 1$ , and  $Q(\vartheta) = q(\vartheta/\theta)/\theta^2$ . Furthermore, we choose the normalization such that

$$2\pi \int_0^\theta d\vartheta \vartheta Q(\vartheta) = 2\pi \int_0^1 dx x q(x) = 1. \quad (3.11)$$

A set of weight functions which satisfy (3.6) and (3.11) is

$$u(x) = \frac{(\ell + 2)^2}{\pi} (1 - x^2)^\ell \left( \frac{1}{\ell + 2} - x^2 \right), \quad (3.12)$$

which peak at  $x = 0$  and go to zero with order  $\ell$  as  $x \rightarrow 1$ . Correspondingly,

$$q(x) = \frac{(1 + \ell)(2 + \ell)}{\pi} x^2 (1 - x^2)^\ell. \quad (3.13)$$

Then defining

$$\begin{aligned}
 I_\ell(\eta) &:= \frac{(\ell+2)^2}{\pi} \int_0^1 dx x (1-x^2)^\ell \left( \frac{1}{\ell+2} - x^2 \right) J_0(\eta x) \\
 &= \frac{2^\ell \Gamma(\ell+3)}{\pi} \eta^{-(\ell+1)} J_{3+\ell}(\eta),
 \end{aligned}
 \tag{3.14}$$

we can write the dispersion as

$$\langle M_{\text{ap}}^2(\theta) \rangle = 2\pi \int_0^\infty ds s P_\kappa(s) [I_\ell(s\theta)]^2.
 \tag{3.15}$$

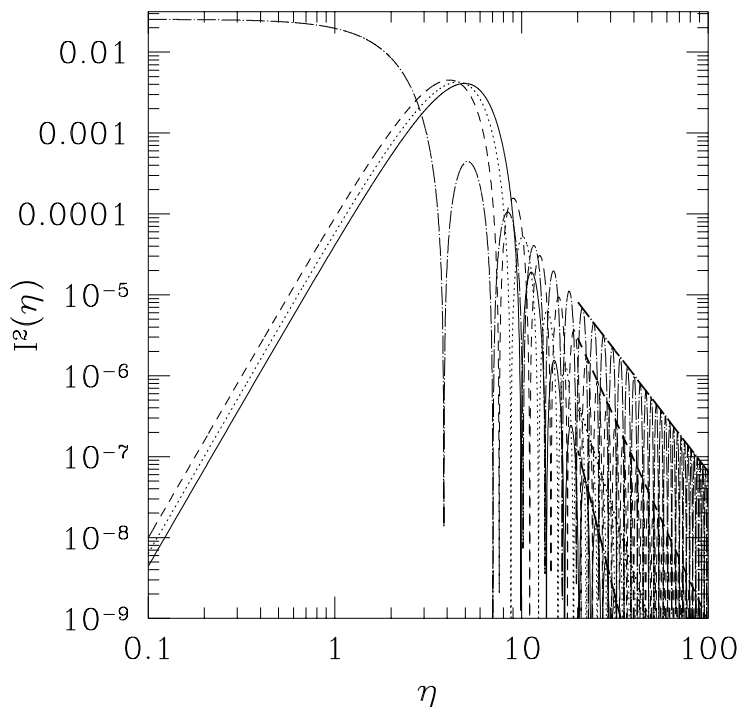


**Fig. 2.** The filter function  $I_\ell^2(\eta)$  in the dispersion of  $M_{\text{ap}}$  for three different value of the  $\ell$ :  $\ell = 1$  (dashed curve),  $\ell = 2$  (dotted curve), and  $\ell = 3$  (solid curve). For comparison, the corresponding filter function for top-hat filtering  $I_{\text{TH}}^2(\eta)$  is also plotted (dashed-dotted curve). For larger values of  $\eta$ , all functions rapidly oscillate, owing to the Bessel functions. For clarity, we have therefore plotted the amplitude of these oscillations as corresponding thick curves

We have plotted the filter function  $I_\ell^2(\eta)$  in Fig. 2, for three different values of  $\ell$ . One can see from (3.14) that  $I_\ell(\eta) \propto \eta^2$  for small  $\eta$ , and that for large  $\eta$ , the function  $I_\ell(\eta)$  oscillates with an amplitude  $\propto \eta^{-(\ell+3/2)}$ . Hence, the filter function  $I_\ell^2$  behaves like  $\eta^4$  and  $\eta^{-(2\ell+3)}$  in the two respective limits, and is indeed a very localized filter, with a peak at  $\eta \sim 5$  for small  $\ell$ . Hence,  $\langle M_{\text{ap}}^2(\theta) \rangle$  provides an accurate measure of the power spectrum of the projected density field at  $s \sim 5/\theta$ , with little dependence on the local shape of this power spectrum.

We shall compare  $\langle M_{\text{ap}}^2(\theta) \rangle$  with the rms value of the shear averaged over a circular region of angular radius  $\theta$ : let

$$\bar{\gamma}(\theta) := \frac{1}{\pi\theta^2} \int d^2\vartheta \gamma(\vartheta), \quad (3.16)$$

then its dispersion is

$$\langle |\bar{\gamma}|^2(\theta) \rangle = 2\pi \int_0^\infty ds s P_\kappa(s) [I_{\text{TH}}(s\theta)]^2, \quad (3.17)$$

with

$$I_{\text{TH}}(\eta) = \frac{J_1(\eta)}{\pi\eta} \quad (3.18)$$

(cf. Blandford et al. 1991). The dash-dotted curve in Fig. 2 displays  $I_{\text{TH}}^2$  for comparison with  $I_\ell$ . One sees that  $I_{\text{TH}}^2$  is a much broader function which tends towards a constant for  $\eta \rightarrow 0$ , and its amplitude decreases like  $\eta^{-3}$  for large  $\eta$ . Therefore, the shear dispersion  $\langle |\bar{\gamma}|^2 \rangle$  is a much coarser probe of the power spectrum than  $\langle M_{\text{ap}}^2(\theta) \rangle$ .

### 3.3 Results

In Fig. 3 we have plotted the rms values of the  $M_{\text{ap}}$ -statistics (upper panel), as well as that of the mean shear within circles (lower panel). The same cosmological models as in Fig. 1 were used, and we present results both for the linearly evolved cosmic power spectrum (thin curves) and for the fully non-linear evolution (thick curves). Whereas  $\langle |\bar{\gamma}|^2 \rangle^{1/2}$  decreases monotonically with  $\theta$ , the shape of  $\langle M_{\text{ap}}^2 \rangle^{1/2}$  closely reflects the shape of the projected power spectrum  $P_\kappa$  displayed in Fig. 1; this is of course related to the narrowness of the filter  $I_\ell$  shown in Fig. 2. In Fig. 3, and for the figures of the remainder of the paper, we used  $\ell = 1$ , but have checked that changing to  $\ell = 2$  or 3 does not yield qualitatively different results. Compared to the prediction of the linear evolution of the power spectrum, the peak of  $\langle M_{\text{ap}}^2 \rangle^{1/2}$  is shifted to substantially smaller angles; at the same time, the non-linear evolution affects  $\langle M_{\text{ap}}^2 \rangle^{1/2}$  more than  $\langle |\bar{\gamma}|^2 \rangle^{1/2}$ , as the latter picks up power from larger scales which are hardly affected by non-linear evolution.

As can be seen from the figure, the values of  $\langle M_{\text{ap}}^2 \rangle^{1/2}$  are substantially smaller than those of  $\langle |\bar{\gamma}|^2 \rangle^{1/2}$ , at least on scales below one degree. This is related to the fact that at a given angular scale  $\theta$ , the  $M_{\text{ap}}$ -statistics is sensitive to smaller-scale structures than the  $|\bar{\gamma}|$ -statistics, as can be seen in Fig. 2, and so these two rms values should be compared at different ‘effective’ scales. Whereas this difference in magnitude may suggest that the  $M_{\text{ap}}$ -statistics is observationally disfavoured, we shall show in Sect. 5 that it has the advantage that measurements in neighboring fields are nearly uncorrelated.

The dependence of the rms of  $M_{\text{ap}}$  on the source redshift distribution is displayed in Fig. 4, for the same five cosmological models, and two angular scales. The dependence on  $z_s$  is generally weak, in rough agreement with the power law dependence  $z_s^{0.6}$  found by JS for the top-hat filter. The model with cosmological constant shows a stronger growth with  $z_s$ , as distances grow faster with redshift in such models, and thus provide larger path lengths for lensing.

## 4 Three-point $M_{\text{ap}}$ -statistics: skewness

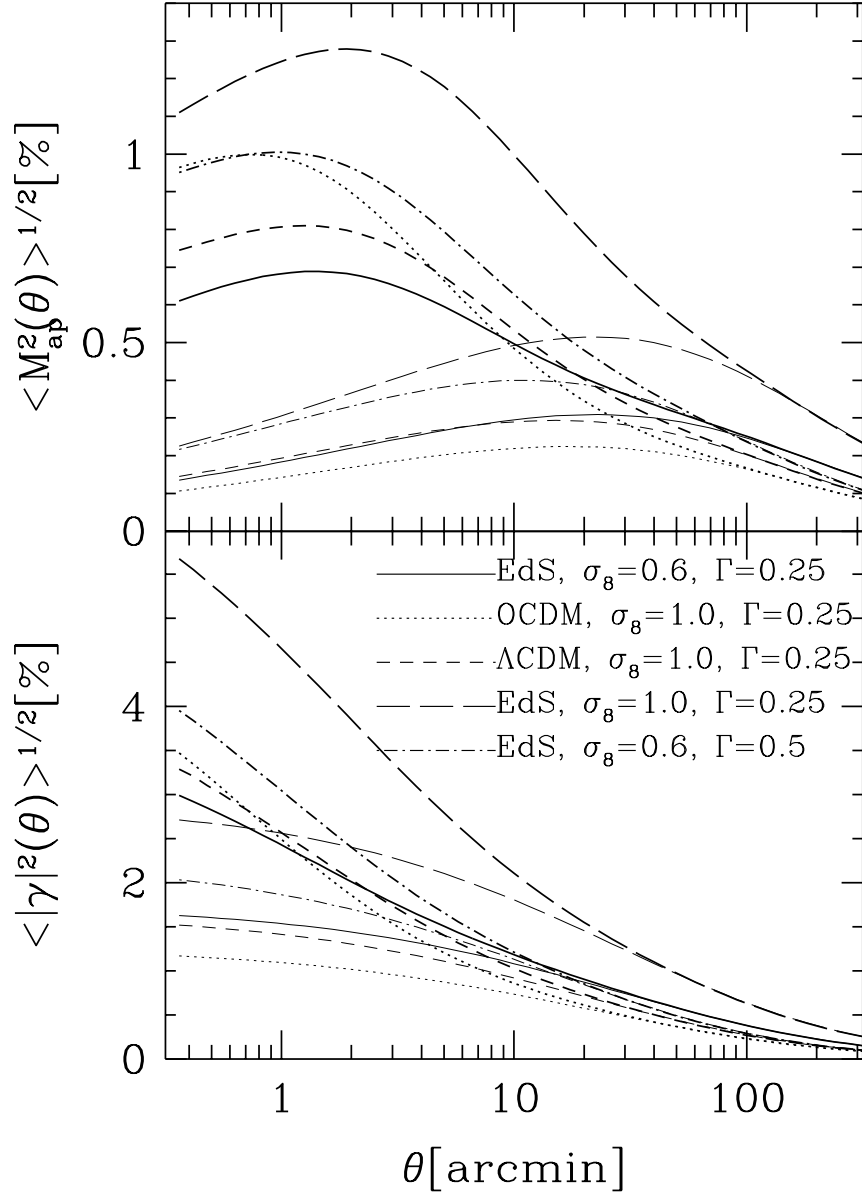


**Fig. 3.** The rms values of the shear are shown vs. filter scale  $\theta$  for the same cosmological models as used in Fig. 1. The upper panel shows the rms value of  $M_{\text{ap}}$  with the filter  $I_1$  defined in (3.14), while the lower panel shows the rms shear computed with a top-hat filter (3.18). Note the different scales in the two panels. The source galaxies are assumed to follow the distribution (2.18), with  $\beta = 1.5$  and  $z_0 = 1$ . The thin curves display the prediction for the rms shear if linear evolution of the density fluctuation spectrum is assumed, whereas the thick curves follow from the fully non-linear evolution of the power spectrum. The results shown in the lower panel are fully equivalent to those of JS, except that they considered a redshift distribution of the form (2.17), and they considered the ‘polarization’ as a measure of net galaxy ellipticity, which in the weak lensing case equals twice the shear

If  $\kappa$  is a Gaussian random field, so is  $M_{\text{ap}}$ , and in particular, the expectation value of the third-order moment of  $M_{\text{ap}}$  would vanish. However, since the nonlinear gravitational evo-

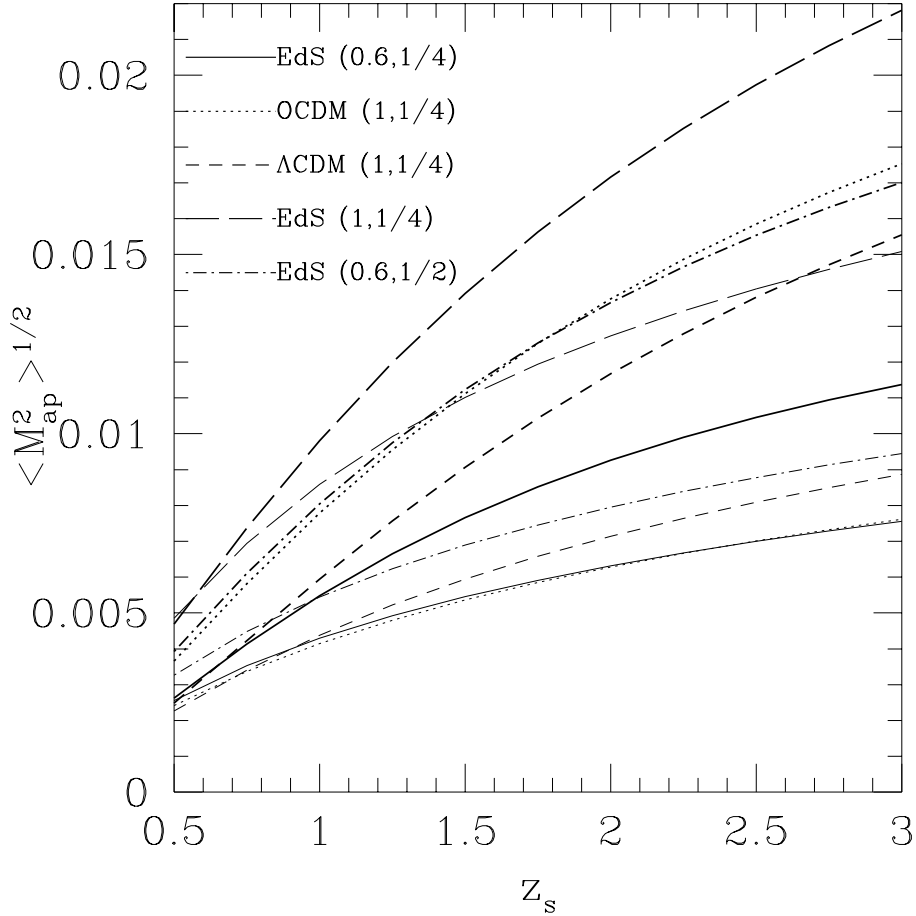


**Fig. 4.** The rms value of  $M_{\text{ap}}$  as a function of source redshift, for the same five cosmological models as in Fig. 1, indicated in the figure; the numbers in parenthesis are  $(\sigma_8, \Gamma)$ . The thick curves are for  $\theta = 1'$ , the thin curves for  $\theta = 10'$ . The fully non-linear evolution of the power spectrum has been used. The sources were assumed to be all at the same redshift  $z_s$

lution of density fluctuations transforms an initially Gaussian field into a non-Gaussian one, this third-order moment is non-zero in general. In fact,  $\langle M_{\text{ap}}^3 \rangle$  is a measure of the non-Gaussianity of the density fluctuations at medium redshifts. Since

$$\begin{aligned}
 \langle M_{\text{ap}}^3(\theta) \rangle &= \int d^2\theta_1 U(\theta_1) \int d^2\theta_2 U(\theta_2) \int d^2\theta_3 U(\theta_3) \langle \kappa(\boldsymbol{\theta}_1) \kappa(\boldsymbol{\theta}_2) \kappa(\boldsymbol{\theta}_3) \rangle \\
 &= \int d^2\theta_1 U(\theta_1) \int d^2\theta_2 U(\theta_2) \int d^2\theta_3 U(\theta_3) \\
 &\quad \times \int \frac{d^2s_1}{(2\pi)^2} e^{i\boldsymbol{\theta}_1 \cdot \mathbf{s}_1} \int \frac{d^2s_2}{(2\pi)^2} e^{i\boldsymbol{\theta}_2 \cdot \mathbf{s}_2} \int \frac{d^2s_3}{(2\pi)^2} e^{i\boldsymbol{\theta}_3 \cdot \mathbf{s}_3} \langle \tilde{\kappa}(\mathbf{s}_1) \tilde{\kappa}(\mathbf{s}_2) \tilde{\kappa}(\mathbf{s}_3) \rangle ,
 \end{aligned} \tag{4.1}$$

the evaluation of the third moment requires the calculation of the three-point correlation function of  $\tilde{\kappa}$ .

The skewness of the projected surface mass density has already been discussed in BvWM. They have calculated the skewness of the projected density field by considering the quasi-linear evolution of the density fluctuations. Below, we shall follow the same procedure to calculate  $\langle M_{\text{ap}}^3 \rangle$ . As was also pointed out by BvWM, even for the strictly

linear evolution of the power spectrum, when the density field conserves its initial Gaussian nature, the observable skewness would not vanish identically. We get back to this point at the end of this section.

#### 4.1 The three-point correlator for $\tilde{\kappa}$

We shall now evaluate this three-point function in terms of the corresponding function of the cosmic density field, i.e., to obtain the analog of (3.4) for the three-point function. For abbreviation, we write (2.14) in the form

$$\kappa(\boldsymbol{\theta}, w) = \int_0^w dw' G(w, w') \delta(f_K(w')\boldsymbol{\theta}, w') , \quad (4.2)$$

with

$$G(w, w') = \frac{3}{2} \left( \frac{H_0}{c} \right)^2 \Omega_d \frac{f_K(w - w') f_K(w')}{f_K(w) a(w')}$$

for  $w' \leq w$ , and zero otherwise. Then,

$$\begin{aligned} & \langle \tilde{\kappa}(\mathbf{s}_1, w_1) \tilde{\kappa}(\mathbf{s}_2, w_2) \tilde{\kappa}(\mathbf{s}_3, w_3) \rangle \\ &= \int d^2\theta_1 e^{-i\mathbf{s}_1 \cdot \boldsymbol{\theta}_1} \int d^2\theta_2 e^{-i\mathbf{s}_2 \cdot \boldsymbol{\theta}_2} \int d^2\theta_3 e^{-i\mathbf{s}_3 \cdot \boldsymbol{\theta}_3} \\ & \times \int_0^{w_1} dv_1 G(w_1, v_1) \int_0^{w_2} dv_2 G(w_2, v_2) \int_0^{w_3} dv_3 G(w_3, v_3) \\ & \times \langle \delta(f_K(v_1)\boldsymbol{\theta}_1, v_1) \delta(f_K(v_2)\boldsymbol{\theta}_2, v_2) \delta(f_K(v_3)\boldsymbol{\theta}_3, v_3) \rangle , \end{aligned} \quad (4.3)$$

where we have inserted the Fourier transforms of  $\tilde{\kappa}$  and used (4.2). Assuming that the largest scale fluctuations are much smaller than the typical distance to a source, the three-point correlation function of  $\delta$  will vanish except when  $v_1 \approx v_2 \approx v_3$ . Thus over the  $v$ -range where  $\langle \delta\delta\delta \rangle$  does not vanish, we can set the  $v$ -arguments in  $G$  to be all the same, and we can also set all  $f_K(v_i)$  equal. Since  $G(w, v) = 0$  if  $v > w$ , the outer  $v$ -integration only extends to  $w_{\min} = \min(w_1, w_2, w_3)$ . Hence, after replacing  $\delta$  by its Fourier transform, one obtains

$$\begin{aligned} & \langle \tilde{\kappa}(\mathbf{s}_1, w_1) \tilde{\kappa}(\mathbf{s}_2, w_2) \tilde{\kappa}(\mathbf{s}_3, w_3) \rangle \\ &= \int d^2\theta_1 e^{-i\mathbf{s}_1 \cdot \boldsymbol{\theta}_1} \int d^2\theta_2 e^{-i\mathbf{s}_2 \cdot \boldsymbol{\theta}_2} \int d^2\theta_3 e^{-i\mathbf{s}_3 \cdot \boldsymbol{\theta}_3} \\ & \times \int_0^{w_{\min}} dv G(w_1, v) G(w_2, v) G(w_3, v) \int dv' \int dv'' \\ & \times \int \frac{d^3k_1}{(2\pi)^3} e^{if_K(v)\boldsymbol{\theta}_1 \cdot \mathbf{k}_1} e^{ik_{13}v} \int \frac{d^3k_2}{(2\pi)^3} e^{if_K(v)\boldsymbol{\theta}_2 \cdot \mathbf{k}_2} e^{ik_{23}v'} \\ & \times \int \frac{d^3k_3}{(2\pi)^3} e^{if_K(v)\boldsymbol{\theta}_3 \cdot \mathbf{k}_3} e^{ik_{33}v''} \langle \tilde{\delta}(\vec{k}_1) \tilde{\delta}(\vec{k}_2) \tilde{\delta}(\vec{k}_3) \rangle , \end{aligned} \quad (4.4)$$

where we have written the 3-dimensional vector  $\vec{k}$  as  $(\mathbf{k}, k_3)$ . The  $\theta_i$ -integrations can now be carried out, each yielding  $(2\pi)^2 \delta_D(\mathbf{s}_i - f_K(v)\mathbf{k}_i)$ . After that, the  $\mathbf{k}_i$ -integrations become trivial. The  $v'$  and  $v''$ -integrations can be carried out yielding delta-functions in  $k_{23}$  and  $k_{33}$ , which are trivially integrated away. One thus finds:

$$\begin{aligned}
\langle \tilde{\kappa}(\mathbf{s}_1, w_1) \tilde{\kappa}(\mathbf{s}_2, w_2) \tilde{\kappa}(\mathbf{s}_3, w_3) \rangle &= \int_0^{w_{\min}} dv G(w_1, v) G(w_2, v) G(w_3, v) \frac{1}{f_K^6(v)} \\
&\times \int \frac{dk_3}{(2\pi)} e^{ik_3 v} \left\langle \tilde{\delta} \left( \frac{\mathbf{s}_1}{f_K(v)}, k_3 \right) \tilde{\delta} \left( \frac{\mathbf{s}_2}{f_K(v)}, 0 \right) \tilde{\delta} \left( \frac{\mathbf{s}_3}{f_K(v)}, 0 \right) \right\rangle (v).
\end{aligned} \tag{4.5}$$

Next, the average of (4.5) over a source redshift distribution is performed. The only point to notice here is the upper limit of integration for  $v$ . Integrating (4.5) over  $\prod \int dw_i p_w(w_i)$  (recall that  $p_w(w) dw = p_z(z) dz$  is the source redshift distribution) gives an expression of the form

$$\begin{aligned}
I &= \int_0^{w_H} dw_1 \int_0^{w_H} dw_2 \int_0^{w_H} dw_3 \int_0^{w_{\min}} dv F \\
&= \int_0^{w_H} dv \int_v^{w_H} dw_1 \int_v^{w_H} dw_2 \int_v^{w_H} dw_3 F.
\end{aligned}$$

In obtaining the second equality we have made use of the fact that the integrand  $F$  is symmetric in  $w_1, w_2, w_3$ , and that  $G(w, v) = 0$  if  $v > w$ . We therefore obtain for the redshift-averaged three-point correlation

$$\begin{aligned}
\langle \tilde{\kappa}(\mathbf{s}_1) \tilde{\kappa}(\mathbf{s}_2) \tilde{\kappa}(\mathbf{s}_3) \rangle &= \frac{27}{8} \left( \frac{H_0}{c} \right)^6 \Omega_d^3 \int_0^{w_H} dw \frac{g^3(w)}{a^3(w) f_K^3(w)} \\
&\times \int \frac{dk_3}{(2\pi)} e^{ik_3 w} \left\langle \tilde{\delta} \left( \frac{\mathbf{s}_1}{f_K(w)}, k_3 \right) \tilde{\delta} \left( \frac{\mathbf{s}_2}{f_K(w)}, 0 \right) \tilde{\delta} \left( \frac{\mathbf{s}_3}{f_K(w)}, 0 \right) \right\rangle,
\end{aligned} \tag{4.6}$$

with  $g(w)$  as defined in (2.16).

## 4.2 Quasi-linear theory of density fluctuations

In order to calculate the triple correlator in (4.6), we shall use quasi-linear perturbation theory, in which the density field  $\delta$  is considered as a ‘small’ quantity and expanded into a perturbation series,  $\delta = \delta^{(1)} + \delta^{(2)} + \dots$ , where  $\delta^{(n)} = \mathcal{O}([\delta^{(1)}]^n)$ . Here,  $\delta^{(1)}$  is the linearly evolved density perturbation,  $\tilde{\delta}^{(1)}(\vec{k}, w) = D_+(w) \tilde{\delta}_0^{(1)}(\vec{k})$ ,  $D_+(w)$  is the linear growth factor, normalized to  $D_+(0) = 1$ , and  $\tilde{\delta}_0^{(1)}(\vec{k})$  is the density perturbation linearly extrapolated to the present epoch. The perturbation series can then be inserted into the continuity equation and the Euler equation, and a closed solution for every order can be obtained in terms of lower-order terms (see, e.g., Fry 1984, Goroff et al. 1986, and references therein). In particular, in an EdS Universe, for the first non-linear term, one obtains

$$\begin{aligned}
\tilde{\delta}^{(2)}(\vec{k}, w) &= D_+^2(w) \int \frac{d^3 k'}{(2\pi)^3} \tilde{\delta}_0^{(1)}(\vec{k}') \tilde{\delta}_0^{(1)}(\vec{k} - \vec{k}') \\
&\times \left[ \frac{5}{7} + \frac{\vec{k}' \cdot (\vec{k} - \vec{k}')}{|\vec{k}'|^2} + \frac{2 \left[ \vec{k}' \cdot (\vec{k} - \vec{k}') \right]^2}{7 |\vec{k}'|^2 |\vec{k} - \vec{k}'|^2} \right].
\end{aligned} \tag{4.7}$$

Bouchet et al. (1992) showed that the  $\vec{k}$ -dependence of this term depends weakly on cosmology, and that it is an excellent approximation to restrict the cosmology dependence solely to the growth factor  $D_+^2(w)$ . In order to calculate  $\langle \tilde{\delta} \tilde{\delta} \tilde{\delta} \rangle$ , we note that the tri-linear correlation of the linear density field vanishes, owing to its assumed Gaussian nature. Thus to lowest order, we have

$$\begin{aligned} \left\langle \tilde{\delta}(\vec{k}_1) \tilde{\delta}(\vec{k}_2) \tilde{\delta}(\vec{k}_3) \right\rangle (w) &= \left\langle \tilde{\delta}^{(1)}(\vec{k}_1, w) \tilde{\delta}^{(1)}(\vec{k}_2, w) \tilde{\delta}^{(2)}(\vec{k}_3, w) \right\rangle \\ &+ 2 \text{ terms obtained from permutation .} \end{aligned} \quad (4.8)$$

Considering only the first term, inserting (4.7), making use of the fact that  $\tilde{\delta}^{(1)}(\vec{k}, w) = D_+(w) \tilde{\delta}_0^{(1)}(\vec{k})$ , and using the relation

$$\begin{aligned} \left\langle \tilde{\delta}^{(1)}(\vec{k}_1) \tilde{\delta}^{(1)}(\vec{k}_2) \tilde{\delta}^{(1)}(\vec{k}_3) \tilde{\delta}^{(1)}(\vec{k}_4) \right\rangle &= \left\langle \tilde{\delta}^{(1)}(\vec{k}_1) \tilde{\delta}^{(1)}(\vec{k}_2) \right\rangle \left\langle \tilde{\delta}^{(1)}(\vec{k}_3) \tilde{\delta}^{(1)}(\vec{k}_4) \right\rangle \\ &+ 2 \text{ terms obtained from permutation} \\ &= (2\pi)^6 \left( P_0(k_1) P_0(k_3) \delta_D(\vec{k}_1 + \vec{k}_2) \delta_D(\vec{k}_3 + \vec{k}_4) \right) + 2 \text{ terms ,} \end{aligned} \quad (4.9)$$

valid for Gaussian fields, we find

$$\begin{aligned} \left\langle \tilde{\delta}^{(1)}(\vec{k}_1) \tilde{\delta}^{(1)}(\vec{k}_2) \tilde{\delta}^{(2)}(\vec{k}_3) \right\rangle (w) &= 2(2\pi)^3 D_+^4(w) P_0(k_1) P_0(k_2) \delta_D(\vec{k}_1 + \vec{k}_2 + \vec{k}_3) \\ &\times \left[ \frac{5}{7} + \frac{1}{2} \left( \frac{1}{|\vec{k}_1|^2} + \frac{1}{|\vec{k}_2|^2} \right) \vec{k}_1 \cdot \vec{k}_2 + \frac{2}{7} \frac{[\vec{k}_1 \cdot \vec{k}_2]^2}{|\vec{k}_1|^2 |\vec{k}_2|^2} \right] . \end{aligned} \quad (4.10)$$

Here,  $P_0(k)$  is the power spectrum of the linearly extrapolated density field. This expression is only one of three terms appearing in (4.8), with the other two being obtained by permutation of the  $\vec{k}_i$ . In order to calculate  $M_{\text{ap}}^3$  according to (4.1), we have to integrate over all  $\mathbf{s}_i$ , and each of the three terms in (4.8) yields the same contribution. Therefore, we can just use (4.10) instead of (4.8), and multiply the result by a factor 3. Then, combining (4.1), (4.6) and (4.10), we obtain

$$\begin{aligned} \langle M_{\text{ap}}^3(\theta) \rangle &= \frac{81}{4} (2\pi)^{-1} \left( \frac{H_0}{c} \right)^6 \Omega_d^3 \int_0^{w_H} dw \frac{g^3(w) D_+^4(w)}{a^3(w) f_K(w)} \\ &\times \int d^2 s_1 P_0 \left( \frac{s_1}{f_K(w)} \right) I(s_1 \theta) \int d^2 s_2 P_0 \left( \frac{s_2}{f_K(w)} \right) I(s_2 \theta) \\ &\times I(|\mathbf{s}_1 + \mathbf{s}_2| \theta) \left[ \frac{5}{7} + \frac{1}{2} \left( \frac{1}{|\mathbf{s}_1|^2} + \frac{1}{|\mathbf{s}_2|^2} \right) \mathbf{s}_1 \cdot \mathbf{s}_2 + \frac{2}{7} \frac{[\mathbf{s}_1 \cdot \mathbf{s}_2]^2}{|\mathbf{s}_1|^2 |\mathbf{s}_2|^2} \right] . \end{aligned} \quad (4.11)$$

### 4.3 Skewness

We define the skewness as

$$S(\theta) := \frac{\langle M_{\text{ap}}^3(\theta) \rangle}{\langle M_{\text{ap}}^2(\theta) \rangle^2} . \quad (4.12)$$

We have calculated  $S(\theta)$  using the results of the preceding subsection. Quasi-linear theory is expected to underestimate  $\langle M_{\text{ap}}^3(\theta) \rangle$ , in particular on scales below  $\sim 20$  arcmin which roughly demarcates the linear and nonlinear regimes. However it has been shown that the quasi-linear theory yields a surprisingly accurate estimate of the skewness of the density field, even in the regime ( $|\delta| \sim 1$ ) where one could not expect the perturbation series to yield reliable results (e.g. Baugh, Gaztañaga & Efstathiou 1995, Colombi, Bouchet & Hernquist 1996, Gaztañaga & Bernardeau 1997). Therefore, we expect that the results



for  $S(\theta)$  as calculated here will provide a good approximation to the true skewness, even on scales down to a few arcminutes. On very small scales with density contrasts much larger than 1, the skewness of the density measured in N-body simulations is indeed larger than the perturbation theory value, but by no more than a factor of two (Baugh et al. 1995, Colombi et al. 1996).

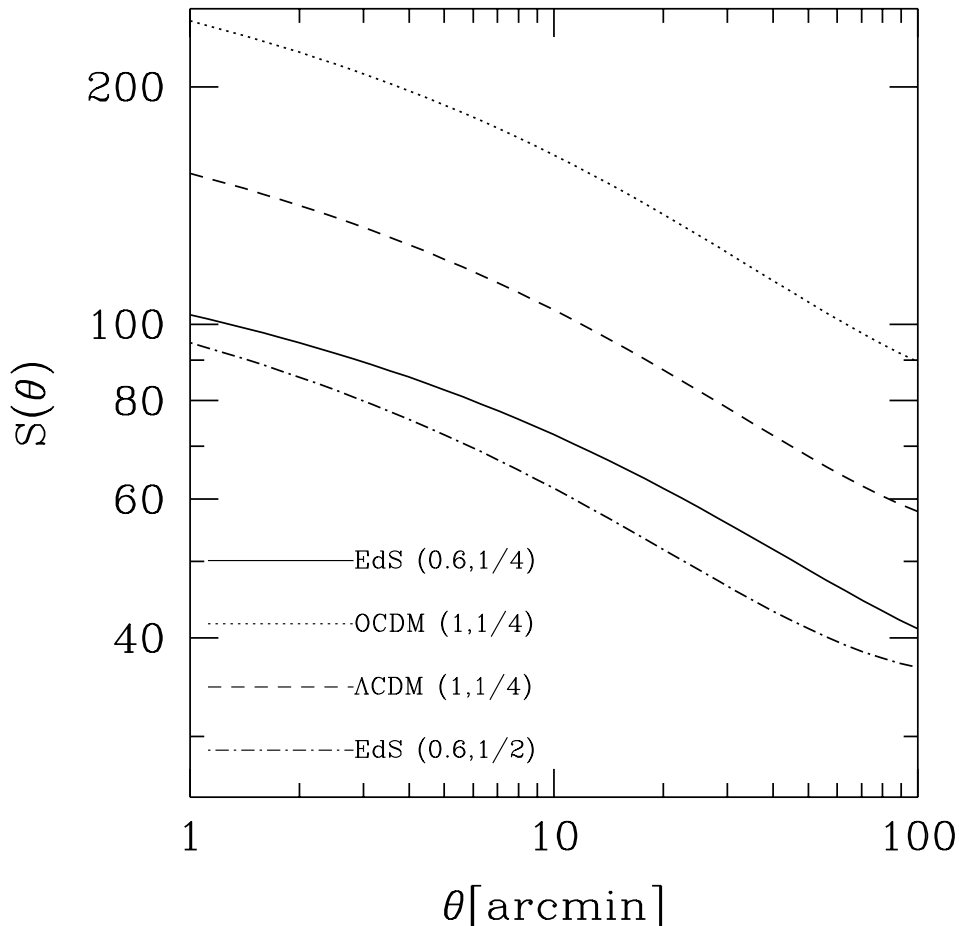


**Fig. 5.** The skewness, as defined in (4.12), as a function of filter scale  $\theta$ , for four cosmological models. Since the skewness as calculated from quasi-linear theory is independent of the normalization of the power spectrum, the two EdS models with the same  $\Gamma$  yield the same  $S(\theta)$  curves. The sources were distributed according to (2.18), with  $z_0 = 1$  and  $\beta = 1.5$ , and the filter with  $\ell = 1$  was used

In Fig. 5 we have plotted the skewness as a function of angular scale, for various cosmological models. Going from an EdS model to an open model, the skewness increases by more than a factor of two, with the spatially flat  $\Lambda$  model taking intermediate values. The two EdS models with different power spectra have only slightly different skewness. This result is in full agreement with BvWM, who found that the skewness is a fairly sensitive probe for the cosmological model, to a large degree independent of the exact shape of the power spectrum. The skewness on an angular scale of  $5'$  is plotted in Fig. 6, for cosmological models with  $\Omega_v = 0$ , and flat cosmologies ( $\Omega_v = 1 - \Omega_d$ ), and two different shape parameters  $\Gamma$  of the power spectrum, as a function of  $\Omega_d$ . The two panels are for different source redshift distributions. Again we see that the variation of  $S$  with

the cosmological parameters is much stronger than with the shape of the power spectrum. And by definition  $S$  is independent of the normalization  $\sigma_8$  of the power spectrum, at least in perturbation theory, where it is the ratio of two terms, each of  $\mathcal{O}\left([\delta^{(1)}]^4\right)$ . We therefore conclude that the skewness is a powerful discriminator between different cosmological models.

Since  $\langle M_{\text{ap}}^3 \rangle$  contains a factor  $\Omega_{\text{d}}^3$ , and  $\langle M_{\text{ap}}^2 \rangle$  has a factor  $\Omega_{\text{d}}^2$ , one expects that to leading order,  $S \propto \Omega_{\text{d}}^{-1}$ . As can be seen from Fig. 6,  $S$  follows this expectation rather closely for the models with  $\Omega_{\text{v}} = 0$ . For flat cosmologies, however, these  $\Omega_{\text{d}}$  factors are no longer the dominant terms in the dependence of  $S$  on  $\Omega_{\text{d}}$ . The dependence on  $\Omega_{\text{d}}$  is weakened due to the distance factors in the integrands for  $\langle M_{\text{ap}}^3 \rangle$  and  $\langle M_{\text{ap}}^2 \rangle$ .

Up to now, we have considered the skewness as it arises due to the quasi-linear evolution of the density field which transforms an initially Gaussian field into a non-Gaussian one. The linear density field would not cause any skewness in the frame of the approximations used up to now. Nevertheless, even in the case of Gaussian density fluctuations, the observable skewness would not be identically zero, owing to the following three effects: (i) Light rays do not propagate along ‘straight’ lines, but are deflected. Therefore, the separation vector  $\mathbf{x}(\boldsymbol{\theta}, w)$  deviates from  $f_K(w)\boldsymbol{\theta}$ . This deviation from the ‘Born approximation’ leads to a non-vanishing skewness. (ii) In the transition from (2.9) to (2.10), in addition to the Born approximation the matrix  $\mathcal{A}$  on the right-hand-side of (2.9) was approximated by the unit matrix; in that way, the leading order term (in  $\Phi$ ) of the propagation matrix was obtained. The next order term, which describes the coupling between lens planes, yields a non-vanishing skewness. These two effects have been quantitatively analyzed in BvWB for the skewness of the projected density field, where it was shown that they are small compared to the expression obtained from quasi-linear density evolution. (iii) The fact that the image ellipticity is not an unbiased estimator for the shear  $\gamma$ , but for the reduced shear  $g = \gamma/(1 - \kappa)$ , implies that a Gaussian density field can produce a finite skewness to the extent that the weak lensing condition  $\kappa \ll 1$  is no longer valid, and that we have to consider the term  $\gamma^{(1)}\kappa^{(1)}$ . We shall consider all three effects in the Appendix. All three effects yield contributions to  $\langle M_{\text{ap}}^3 \rangle$  which are proportional to the square of the power spectrum  $P_0(k)$ , as is the case for the leading term considered here. Therefore, there is no a priori reason to expect that these ‘correction’ terms are much smaller than (4.11). As it turns out, however, these correction terms amount to  $\sim 5\%$  of the leading term (4.11), and may therefore be safely neglected presently.

A final point concerns the redshift distribution of the sources. Fig. 6 shows that the source redshift dependence of  $S$  is rather large, as pointed out by BvWM. This is a potential problem for two reasons: (1) First, it means that in order to compare an observed skewness with theoretical calculations, we have to know the redshift distribution fairly precisely. Since the likely sources are very faint, a complete spectroscopic survey to the corresponding magnitude limits is not available, but progress in the method of photometric redshifts may yield sufficiently accurate estimates of the required distribution. (2) The magnification bias changes the redshift distribution of the observed galaxy images in a way which depends on the local value of the magnification. The observed skewness is sensitive to this. It is not the aim of this paper to discuss these points. A rough estimate of the second point shows that the magnification bias is negligible, but a detailed and systematic analysis of these effects remains to be done.

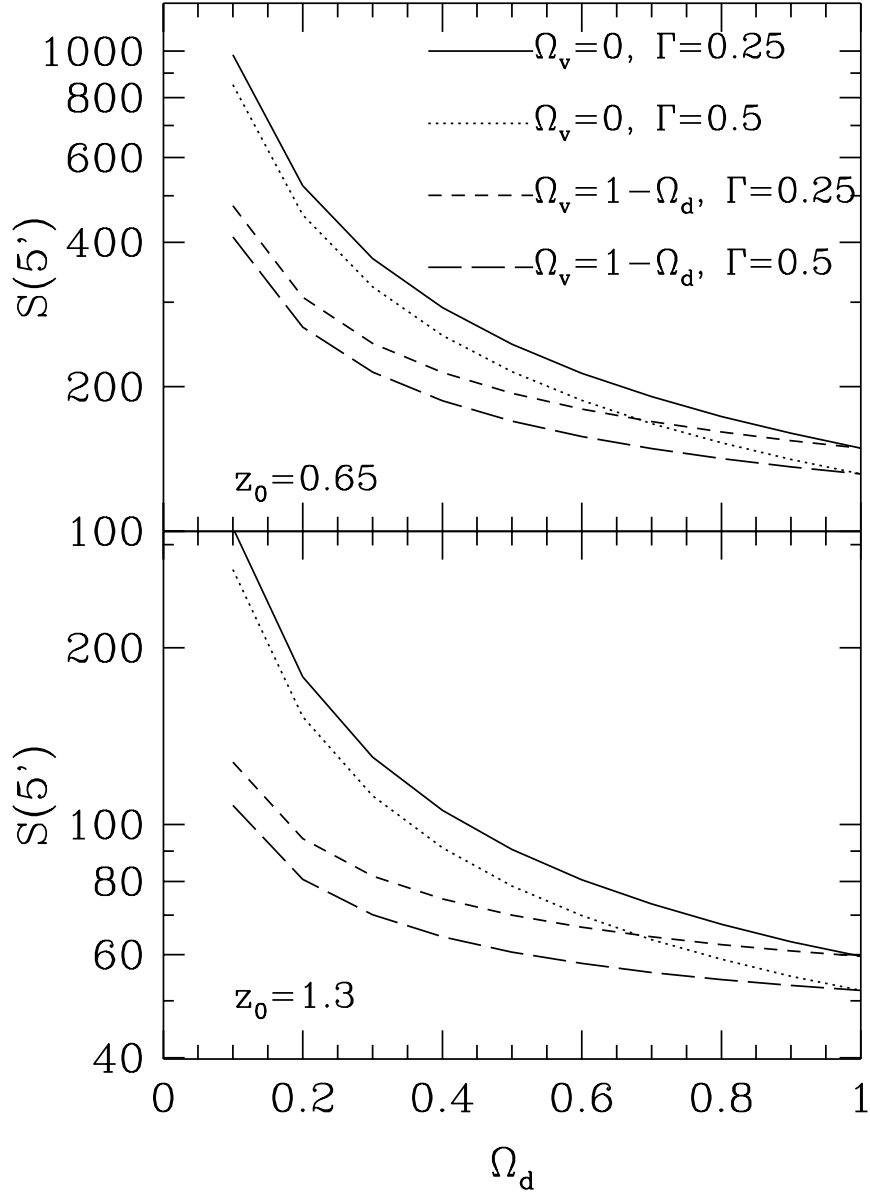


**Fig. 6.** The skewness, as defined in (4.12), as a function of  $\Omega_d$ , for vanishing cosmological constant  $\Omega_v = 0$ , and for flat Universes,  $\Omega_v = 1 - \Omega_d$ . For both cases, two values of the shape parameter  $\Gamma$  were considered. The redshift distribution of the sources was assumed to follow (2.18), with  $\beta = 1.5$ , and  $z_0 = 0.65$  (upper panel) and  $z_0 = 1.3$  (lower panel), corresponding to a mean redshift of about one and two, respectively. As can be seen, the dependence of  $S$  on the cosmological parameters is considerably stronger than the dependence on the shape of the power spectrum

## 5 Practical estimates

We shall now consider some practical estimators for the  $M_{\text{ap}}$ -statistics, and their dispersion. The results of this section yield an estimate of the observations necessary to measure  $\langle M_{\text{ap}}^2 \rangle$  with given precision.

## 5.1 Dispersion for a single field

Consider first a single circular field of angular radius  $\theta$ , in which  $N$  galaxies are observed at positions  $\boldsymbol{\theta}_i$  with complex ellipticity  $\epsilon_i$ . In the case of weak lensing,  $\kappa \ll 1$ , the transformation from the intrinsic ellipticity  $\epsilon^{(s)}$  to the observed one is simply  $\epsilon = \gamma + \epsilon^{(s)}$ . Since the intrinsic orientation of galaxies is random,  $\epsilon$  is an unbiased estimator of the local shear. Defining in analogy to (3.9) the tangential component of the ellipticity of a galaxy at  $\boldsymbol{\theta}_i = (\theta_i \cos \varphi_i, \theta_i \sin \varphi_i)$  by

$$\epsilon_{ti} = -\mathcal{R}e(\epsilon_i e^{-2i\varphi_i}) , \quad (5.1)$$

then  $\epsilon_{ti}$  is an unbiased estimator of  $\gamma_t(\boldsymbol{\theta}_i) \equiv \gamma_{ti}$ . In terms of the observable image ellipticities, we define the estimator

$$M := \frac{(\pi\theta^2)^2}{N(N-1)} \sum_{i,j \neq i}^N Q_i Q_j \epsilon_{ti} \epsilon_{tj} , \quad (5.2)$$

where  $Q_i \equiv Q(\boldsymbol{\theta}_i)$ , which in turn is defined in (3.8), and the sum is taken only over terms with  $i \neq j$ . The expectation value of  $M$  is obtained by three averaging processes: averaging over the intrinsic ellipticity distribution, averaging over the galaxy positions, and the ensemble average. We denote the first of these processes by the operator  $\mathbf{A}$ , and the second by  $\mathbf{P}$ ; these two operators commute. Then,

$$\mathbf{A}(\epsilon_{ti} \epsilon_{tj}) = \mathbf{A}\left([\gamma_{ti} + \epsilon_{ti}^{(s)}][\gamma_{tj} + \epsilon_{tj}^{(s)}]\right) = \gamma_{ti} \gamma_{tj} + \frac{\sigma_\epsilon^2}{2} \delta_{ij} , \quad (5.3)$$

since  $\mathbf{A}(\epsilon_{ti}^{(s)}) = 0$ , owing to the random intrinsic orientation; here,  $\sigma_\epsilon$  is the dispersion of the intrinsic ellipticity distribution. The term with  $\sigma_\epsilon^2$  is divided by 2 as we want the dispersion of only one component of the complex ellipticity. In (5.3) we also used the fact that the intrinsic ellipticity is uncorrelated with the shear. Note that the second term in (5.3) does not appear in the sum of (5.2). The operator  $\mathbf{P}$  which averages over galaxy positions is defined as

$$\mathbf{P}(X) = \left( \prod_{i=1}^N \int \frac{d^2\theta_i}{\pi\theta^2} \right) X , \quad (5.4)$$

so that

$$\mathbf{P}\left(\sum_{i,j \neq i}^N Q_i Q_j \gamma_{ti} \gamma_{tj}\right) = \frac{N(N-1)}{(\pi\theta^2)^2} \int d^2\theta_1 Q(\theta_1) \int d^2\theta_2 Q(\theta_2) \gamma_t(\boldsymbol{\theta}_1) \gamma_t(\boldsymbol{\theta}_2) , \quad (5.5)$$

because the sum yields  $N(N-1)$  equal terms. The expectation value  $\mathbf{E}(M)$  of  $M$  then becomes:

$$\mathbf{E}(M) \equiv \langle \mathbf{P}(\mathbf{A}(M)) \rangle = \int d^2\theta_1 Q(\theta_1) \int d^2\theta_2 Q(\theta_2) \langle \gamma_t(\boldsymbol{\theta}_1) \gamma_t(\boldsymbol{\theta}_2) \rangle = \langle M_{\text{ap}}^2 \rangle . \quad (5.6)$$

Hence,  $M$  is an unbiased estimator for  $\langle M_{\text{ap}}^2 \rangle$ .

Next, we consider the dispersion of this estimator,

$$\sigma^2(M) = \mathbb{E}(M^2) - [\mathbb{E}(M)]^2, \quad (5.7)$$

with

$$M^2 = \frac{(\pi\theta^2)^4}{N^2(N-1)^2} \sum_{i,j \neq i}^N Q_i Q_j \epsilon_{ti} \epsilon_{tj} \sum_{k,l \neq k}^N Q_k Q_l \epsilon_{tk} \epsilon_{tl}. \quad (5.8)$$

Starting with performing the average over the intrinsic ellipticity distribution, we find

$$\begin{aligned} \mathbb{A}(\epsilon_{ti} \epsilon_{tj} \epsilon_{tk} \epsilon_{tl}) &= \gamma_{ti} \gamma_{tj} \gamma_{tk} \gamma_{tl} + \mathbb{A} \left( \epsilon_{ti}^{(s)} \epsilon_{tj}^{(s)} \epsilon_{tk}^{(s)} \epsilon_{tl}^{(s)} \right) \\ &+ \frac{\sigma_\epsilon^2}{2} (\gamma_{ti} \gamma_{tj} \delta_{kl} + \gamma_{ti} \gamma_{tk} \delta_{jl} + \gamma_{ti} \gamma_{tl} \delta_{jk} + \gamma_{tj} \gamma_{tk} \delta_{il} + \gamma_{tj} \gamma_{tl} \delta_{ik} + \gamma_{tk} \gamma_{tl} \delta_{ij}). \end{aligned} \quad (5.9)$$

Owing to the restrictions in the sums of (5.8), the first and last term in the second parenthesis do not contribute.

To evaluate the position-average over the first term in (5.9), we have to consider three different cases: (a) all four indices  $i, j, k, l$  are different; (b) one of the second pair of indices  $k, l$  is equal to one of the first pair  $i, j$ ; (c) both indices in the second pair are equal to those in the first. These cases occur in the sum of (5.8) in  $N(N-1)(N-2)(N-3)$ ,  $4N(N-1)(N-2)$ , and  $2N(N-1)$  terms, respectively. Therefore,

$$\begin{aligned} &\mathbb{P} \left( \sum_{i,j \neq i}^N \sum_{k,l \neq k}^N Q_i Q_j Q_k Q_l \gamma_{ti} \gamma_{tj} \gamma_{tk} \gamma_{tl} \right) \\ &= \frac{N(N-1)(N-2)(N-3)}{(\pi\theta^2)^4} M_{\text{ap}}^4 + \frac{4N(N-1)(N-2)}{(\pi\theta^2)^3} M_{\text{ap}}^2 \int d^2\vartheta Q^2(\vartheta) \gamma_t^2(\vartheta) \\ &+ \frac{2N(N-1)}{(\pi\theta^2)^2} \left( \int d^2\vartheta Q^2(\vartheta) \gamma_t^2(\vartheta) \right)^2 \end{aligned} \quad (5.10)$$

For the second term in (5.9), we note that since  $i \neq j, k \neq l$ ,  $\mathbb{A} \left( \epsilon_{ti}^{(s)} \epsilon_{tj}^{(s)} \epsilon_{tk}^{(s)} \epsilon_{tl}^{(s)} \right)$  contributes to the sum in (5.8) only for  $k = i$  and  $l = j$ , or  $k = j$  and  $l = i$ . There are  $2N(N-1)$  such terms. Hence,

$$\mathbb{P} \left( \sum_{i,j \neq i}^N \sum_{k,l \neq k}^N Q_i Q_j Q_k Q_l \mathbb{A} \left( \epsilon_{ti}^{(s)} \epsilon_{tj}^{(s)} \epsilon_{tk}^{(s)} \epsilon_{tl}^{(s)} \right) \right) = \frac{2N(N-1)}{(\pi\theta^2)^4} \left( \frac{\sigma_\epsilon^2}{2} \right)^2 G^2, \quad (5.11)$$

where we have defined

$$G = \pi\theta^2 \int d^2\vartheta Q^2(\vartheta). \quad (5.12)$$

Finally, each of the four terms in the last term of (5.9) which contribute to the sum in (5.8) yield the same result when averaged over position. Considering one of these,

$$\begin{aligned} &\mathbb{P} \left( \sum_{i,j \neq i}^N \sum_{k,l \neq k}^N Q_i Q_j Q_k Q_l \gamma_{ti} \gamma_{tk} \delta_{jl} \right) = \mathbb{P} \left( \sum_{j,i \neq j, k \neq j}^N Q_i Q_j^2 Q_k \gamma_{ti} \gamma_{tk} \right) \\ &= \frac{N(N-1)(N-2)}{(\pi\theta^2)^4} M_{\text{ap}}^2 G + \frac{N(N-1)}{(\pi\theta^2)^3} G \int d^2\vartheta Q^2(\vartheta) \gamma_t^2(\vartheta), \end{aligned} \quad (5.13)$$

where the first term comes from terms with  $i \neq k$ , and the second are those from  $i = k$ . Collecting terms, and taking the ensemble average yields for the dispersion

$$\begin{aligned} \sigma^2(M) &= \frac{(N-2)(N-3)}{N(N-1)} \langle M_{\text{ap}}^4 \rangle + \frac{4(N-2)}{N(N-1)} \langle M_{\text{ap}}^2 M_s^2 \rangle \\ &+ \frac{2}{N(N-1)} \langle M_s^4 \rangle + \frac{2(N-2)}{N(N-1)} \sigma_\epsilon^2 G \langle M_{\text{ap}}^2 \rangle \\ &+ \frac{2}{N(N-1)} \sigma_\epsilon^2 G \langle M_s^2 \rangle + \frac{1}{2N(N-1)} \sigma_\epsilon^4 G^2 - \langle M_{\text{ap}}^2 \rangle^2, \end{aligned} \quad (5.14)$$

with

$$M_s^2 := \pi\theta^2 \int d^2\vartheta Q^2(\vartheta) \gamma_t^2(\vartheta). \quad (5.15)$$

Note that the dispersion contains three different sources of noise: the contribution due to the finite width of the intrinsic ellipticity distribution, the ‘cosmic variance’, and the noise due to the finite number of randomly located galaxy images. The latter effect is contained in the terms which include  $M_s$ . However, this source of noise is never dominant: since the magnitude of  $M_s^2$  will be comparable with that of  $M_{\text{ap}}^2$ , the second term in (5.14) is smaller by a factor  $1/N$  than the first, and smaller by a factor  $2GM_s^2/\sigma_\epsilon^2$  than the fourth term. Similar estimates are valid for the other two terms containing  $M_s^2$ . Thus, by dropping terms containing  $M_s$  and taking  $N \gg 1$ , we find

$$\sigma^2(M) \approx \mu_4 \langle M_{\text{ap}}^2 \rangle^2 + \left( \frac{\sigma_\epsilon^2 G}{\sqrt{2}N} + \sqrt{2} \langle M_{\text{ap}}^2 \rangle \right)^2, \quad (5.16)$$

where  $\mu_4$  is the kurtosis of  $M_{\text{ap}}$ ,  $\mu_4 = \langle M_{\text{ap}}^4 \rangle / \langle M_{\text{ap}}^2 \rangle^2 - 3$ , which vanishes if  $M_{\text{ap}}$  is distributed like a Gaussian. We note that  $G$  is a factor of order unity; if we choose the weight function (3.12 & 13), we obtain

$$G = \frac{(1+\ell)(2+\ell)^2}{(1+2\ell)(3+2\ell)}, \quad (5.17)$$

which yields  $G = 6/5$ ,  $48/35$ , and  $100/63$  for  $\ell = 1, 2, 3$ . In order to see whether the cosmic variance or the intrinsic ellipticity distribution dominates the noise, we consider the ratio

$$\rho = \frac{2 \langle M_{\text{ap}}^2 \rangle N}{\sigma_\epsilon^2 G} = \frac{1500\pi}{G} \langle M_{\text{ap}}^2(\theta) \rangle \left( \frac{\theta}{1 \text{ arcmin}} \right)^2 \left( \frac{\sigma_\epsilon}{0.2} \right)^{-2} \left( \frac{n}{30 \text{ arcmin}^{-2}} \right), \quad (5.18)$$

where  $n = N/(\pi\theta^2)$  is the mean density of galaxy images. If  $\rho \ll 1$ , the intrinsic ellipticity distribution contributes mostly to the noise, whereas in the other case, the cosmic variance is the dominating factor. In this discussion the kurtosis term in (5.16) has been ignored.

The coefficient  $\rho$  is plotted in the upper panel of Fig. 7, as a function of  $\theta$ , for the same cosmological models as considered before. One sees that for filter scales exceeding a few arcminutes, the intrinsic ellipticity distribution of galaxies is no longer the dominant source of noise, but the ‘cosmic variance’ will start to dominate.

## 5.2 Dispersion for an ensemble of fields

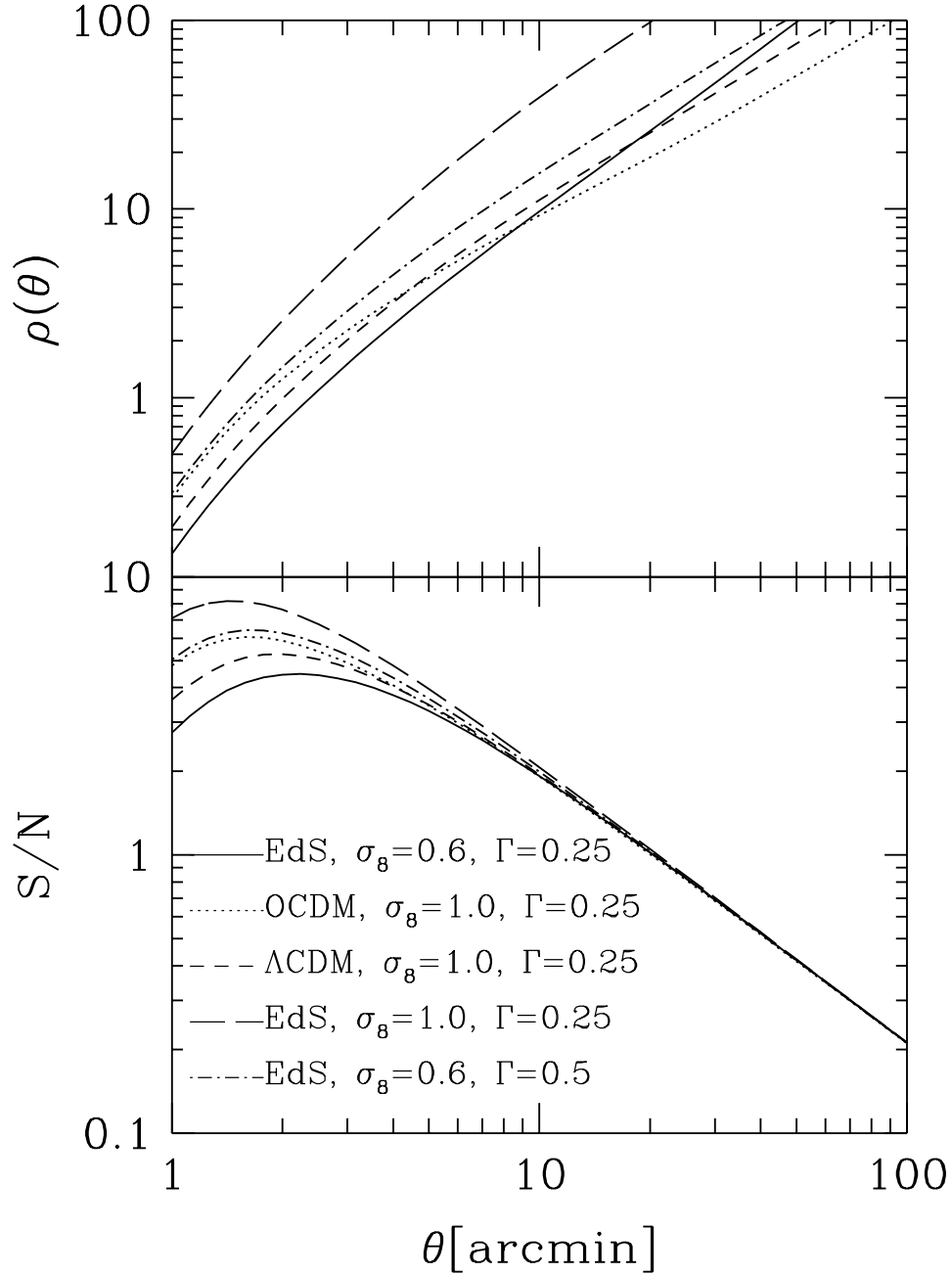


**Fig. 7.** The upper panel displays the quantity  $\rho$  – see (5.18) – as a function of angle  $\theta$ , which describes the relative importance of the cosmic variance relative to the intrinsic galaxy ellipticity dispersion, for the same cosmological models as shown in Fig. 1. In this figure, we have set  $\sigma_\epsilon = 0.2$  and  $n = 30 \text{ arcmin}^{-2}$ ; the dependence on these two quantities can be seen from (5.18). Also, we have used the filter with  $\ell = 1$ . For all cosmological models considered here, the cosmic shear dominates for angular scales above a few arcminutes. In the lower panel, we plot the signal-to-noise ratio (5.22) for the dispersion on angular scale  $\theta$ , for the case that one has a square field of length  $L = 1$  degree available, and that this field is densely covered with circles of radius  $\theta$ , so that  $N_f = (L/2\theta)^2$ . We have assumed zero kurtosis for this plot. The signal-to-noise ratio at fixed  $\theta$  is proportional to  $L$ . Parameters were chosen as in the upper panel. For both panels, the redshift distribution was chosen according to (2.18), with  $z_0 = 1$  and  $\beta = 1.5$ , and the fully non-linear power spectrum was used

Obviously, from observing a single field with radius  $\theta$ , no reliable estimate for  $\langle M_{\text{ap}}^2(\theta) \rangle$  can be obtained. We next consider a sample of  $N_f$  fields, and assume that they are spatially sufficiently well separated so that the shear in one field is statistically independent of that in the others. In that case, an unbiased estimator of  $\langle M_{\text{ap}}^2 \rangle$  is provided by

$$\mathcal{M} = \left( \sum_{n=1}^{N_f} a_n \right)^{-1} \sum_{n=1}^{N_f} a_n M_n, \quad (5.19)$$

where  $M_n$  is the estimator (5.2) in a single field, and the  $a_n$  are weight factors. It is easy to show that the dispersion of  $\mathcal{M}$  is minimized if  $a_n \propto \sigma^{-2}(M_n)$ , in which case it becomes

$$\sigma^2(\mathcal{M}) = \left( \sum_{n=1}^{N_f} \sigma^{-2}(M_n) \right)^{-2} \sum_{n=1}^{N_f} \sigma^{-2}(M_n). \quad (5.20)$$

If all  $N_f$  fields contain the same number of galaxies, then, as expected,

$$\sigma(\mathcal{M}) = \frac{\sigma(M)}{\sqrt{N_f}}. \quad (5.21)$$

Combining (5.16) with (5.18) and (5.21), we find for the signal-to-noise ratio for a measurement of  $\langle M_{\text{ap}}^2 \rangle$ :

$$\frac{S}{N} := \frac{\langle m^2 \rangle}{\sigma(\mathcal{M})} = \frac{\sqrt{N_f}}{\sqrt{\mu_4 + 2 \left(1 + \frac{1}{\rho}\right)^2}}. \quad (5.22)$$

The question of how far two fields have to be separated before they can be considered statistically independent can be investigated by considering the correlation between the values of  $M_{\text{ap}}$  in two fields of angular radius  $\theta_1$  and  $\theta_2$ , separated by  $\Delta\theta$ . We consider the correlation coefficient

$$r_{\text{corr}}(\theta_1, \theta_2; \Delta\theta) := \frac{\langle M_{\text{ap}}(\theta_1) M_{\text{ap}}(\theta_2) \rangle (\Delta\theta)}{\sqrt{\langle M_{\text{ap}}^2(\theta_1) \rangle \langle M_{\text{ap}}^2(\theta_2) \rangle}}, \quad (5.23)$$

which can be easily calculated with (3.5) and (3.2) to yield

$$r_{\text{corr}}(\theta_1, \theta_2; \Delta\theta) = \frac{2\pi}{\sqrt{\langle M_{\text{ap}}^2(\theta_1) \rangle \langle M_{\text{ap}}^2(\theta_2) \rangle}} \int_0^\infty ds s P_\kappa(s) J_0(s \Delta\theta) I_\ell(s\theta_1) I_\ell(s\theta_2). \quad (5.24)$$

This can be compared with the correlation of the mean shear  $\bar{\gamma}(\theta)$  as defined in (3.16), for which the corresponding correlation coefficient is the same as in (5.24) with  $I_\ell(sR)$  replaced by  $I_{\text{TH}}(s\theta)$ . In Fig. 8 we have plotted  $r_{\text{corr}}$  for various values of  $\theta_1$ ,  $\theta_2$  and  $\Delta\theta$ , both for the  $M_{\text{ap}}$ -statistics and for  $\bar{\gamma}$ . From the figure it can be easily seen that the  $M_{\text{ap}}$ -statistics decorrelates very quickly. For example, considering two circles of equal radius, such that they just touch (so that  $\theta_1 = \theta_2 = \Delta\theta/2$ ), we infer from the upper left panel in Fig. 8 that the correlation between the  $M_{\text{ap}}$  measurements in these two apertures is less than 1%! Therefore, if we had a large image, we can place apertures densely on that image and consider the  $M_{\text{ap}}$ -values obtained from each aperture as independent. Also,



for different values of  $\theta_1$  and  $\theta_2$ , the decorrelation is very quick. This property can then be employed for obtaining  $\langle M_{\text{ap}}^2(\theta) \rangle$  from a big image for various angular scales.

Thus, for an image with sidelength  $L$ , we can place  $N_{\text{f}} = (L/2\theta)^2$  nearly independent apertures on this field. Using this estimate, we have plotted S/N, as defined in (5.22), in the lower panel of Fig. 7, assuming  $L = 1$  degree. There we can see that the S/N ratio is larger than one for angular scales below  $20'$ . For different values of  $L$ , one uses the scaling  $S/N \propto L$ . The results of Fig. 7 can be compared with the Fig. 10 of JS which gives the signal-to-noise of the rms shear with a top-hat window.

In contrast to  $M_{\text{ap}}$ ,  $\bar{\gamma}$  decorrelates very slowly, as indicated by the light curves in Fig. 8. This can be traced directly to the shape of the top-hat filter  $I_{\text{TH}}$ , displayed in Fig. 2, which picks up long-scale power of the density field. Therefore, if one wants to measure cosmic shear using  $\bar{\gamma}$ , one has to use data fields which are well separated on the sky.

### 5.3 Alternative estimators

An apparently unrelated estimator for  $\langle M_{\text{ap}}^2 \rangle$  can be obtained from the following consideration: define

$$\hat{\gamma}(\theta) := \int d^2\vartheta U(\vartheta) \gamma(\vartheta), \quad (5.25)$$

where the integral extend over a circle with radius  $\theta$ . This definition is analogous to the one in (3.16), except that a weight function is added. Then

$$\langle \hat{\gamma} \hat{\gamma}^* \rangle = \int d^2\theta' U(\theta') \int d^2\vartheta U(\vartheta) \langle \gamma(\theta') \gamma^*(\vartheta) \rangle. \quad (5.26)$$

Noting that the two-point correlation function of the shear is the same as the two-point correlation function of  $\kappa$  (see, e.g., Blandford et al. 1991), we see that this expression agrees with (3.10), so that

$$\langle M_{\text{ap}}^2(\theta) \rangle = \langle \hat{\gamma}(\theta) \hat{\gamma}^*(\theta) \rangle. \quad (5.27)$$

Hence, a practical estimator for  $\langle M_{\text{ap}}^2 \rangle$  is

$$\hat{M} = \frac{(\pi\theta^2)^2}{N(N-1)} \sum_{i,j \neq i}^N U(\theta_i) U(\theta_j) (\epsilon_{1i}\epsilon_{1j} + \epsilon_{2i}\epsilon_{2j}). \quad (5.28)$$

With calculation similar to those in Sect. 5.1, one can show that indeed  $\hat{M}$  is an unbiased estimator for  $\langle M_{\text{ap}}^2 \rangle$ ; its dispersion in the same approximation as in (5.16) is

$$\sigma^2(\hat{M}) = \hat{\mu}_4 \langle M_{\text{ap}}^2 \rangle^2 + \left( \frac{\sigma_\epsilon^2 \hat{G}}{N} + \sqrt{2} \langle M_{\text{ap}}^2 \rangle \right)^2, \quad (5.29)$$

where  $\hat{\mu}_4$  is the kurtosis of the shear  $\hat{\gamma}$ , and

$$\hat{G} = \pi\theta^2 \int d^2\vartheta U^2(\vartheta) = G, \quad (5.30)$$

where the final equality is valid if  $U$  is chosen as in (3.12). Thus we see that the dispersion of  $\hat{M}$  is very similar to that of  $M$ , except for a factor  $\sqrt{2}$  in the term containing  $\sigma_\epsilon$ .

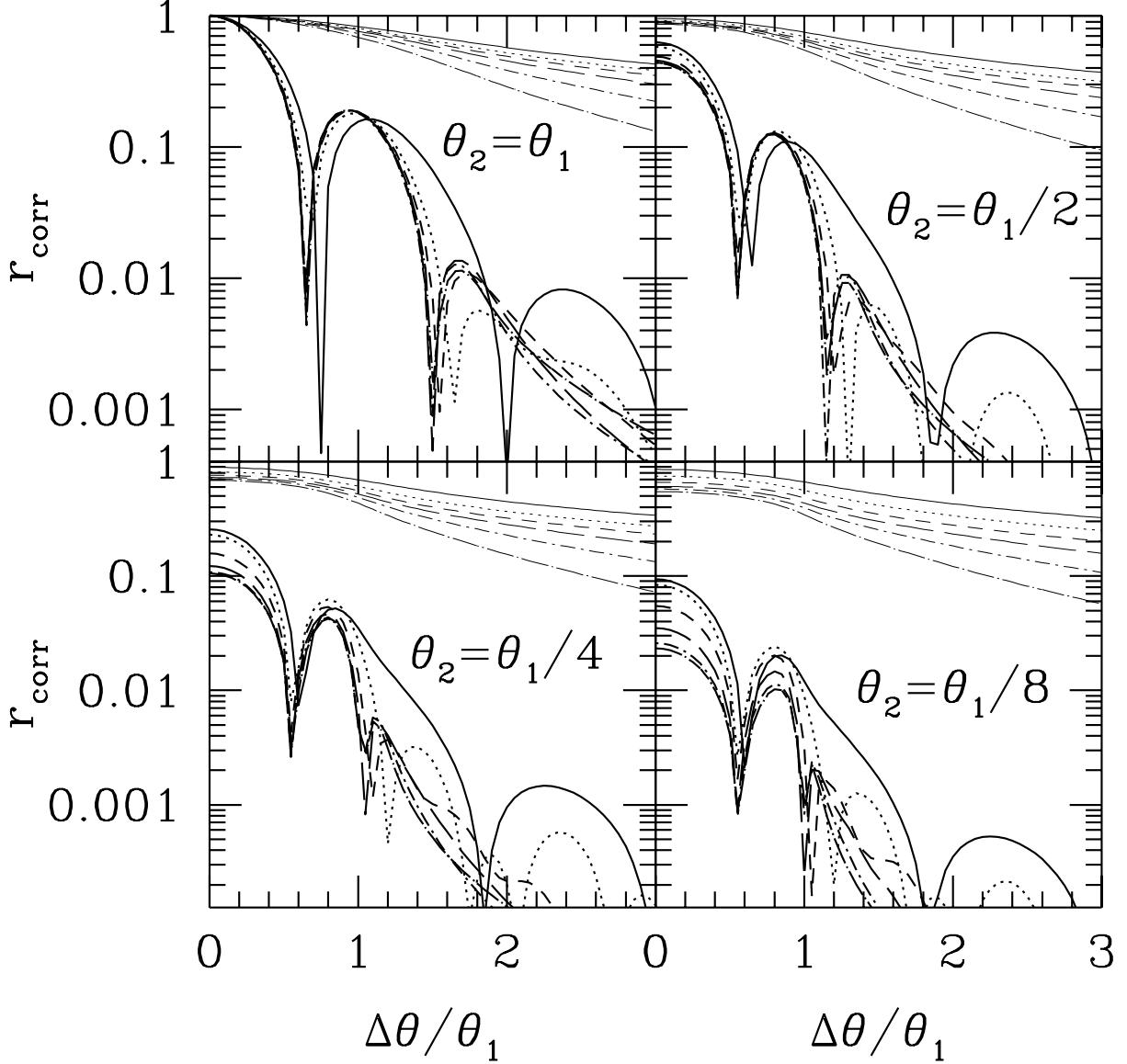


**Fig. 8.** The correlation coefficient  $r_{\text{corr}}(\theta_1, \theta_2; \Delta\theta)$  is plotted as a function of  $\Delta\theta/\theta_1$  (heavy curves). Here,  $\theta_1$  is the larger of the two aperture sizes; the other one is 1, 1/2, 1/4, and 1/8 of the former one in the four different panels. Six curves are drawn in each panel, corresponding to  $\theta_1/\text{arcmin} = 1$  (solid curves), 2 (dotted curves), 4 (short-dashed curves), 8 (long-dashed curves), 16 (short-dashed-dotted curves), and 32 (long-dashed-dotted curves). The light curves in each panel is the corresponding correlation coefficient for the mean shear inside circles,  $\bar{\gamma}(\theta)$ . For this figure, an  $\Omega_d = 1$ ,  $\Omega_v = 0$  universe has been assumed, with  $\sigma_8 = 0.6$  and  $\Gamma = 0.25$ , and the sources were assumed to follow the redshift distribution (2.18) with  $z_0 = 1$  and  $\beta = 1.5$

This difference is due to the fact that in  $\hat{M}$ , two components of  $\epsilon$  are used, each of which carries its dispersion. Hence, for measuring  $\langle M_{\text{ap}}^2(\theta) \rangle$ , one can use the estimators (5.2) and (5.28), where the former should yield a slightly higher signal-to-noise ratio. A comparison between these two estimates can be used to check the integrity of the data and the data analysis procedure.

Another check on the quality of the data can be obtained by noting that

$$M_r := \int d^2\vartheta Q(|\vartheta|) \gamma_r(\vartheta) \quad (5.31)$$

should vanish identically, where  $\gamma_r$  is the radial component of the shear, defined by taking the imaginary part in (3.9) instead of the real part for the tangential component. The fact that  $M_r = 0$  can be shown easily by introducing the Fourier transform of  $\gamma_r$  to obtain a result similar to (A5), with the cosine replaced by a sine; the polar angle integral in (5.31) then yields zero. The estimator

$$\mathcal{M}_r = \sum_{n=1}^{N_f} \left( \frac{(\pi\theta)^2}{N(N-1)} \sum_{i,j \neq i}^N Q_i Q_j \epsilon_{ri} \epsilon_{rj} \right)$$

should therefore yield a value within the dispersion, which is given by  $\sigma(\mathcal{M}_r) = \sigma_\epsilon^2 G / (\sqrt{2N_f} N)$ .

#### 5.4 Practical estimator for $\langle M_{\text{ap}}^3 \rangle$

An obvious estimator for  $\langle M_{\text{ap}}^3(\theta) \rangle$  for a single field is

$$M_3 := \frac{(\pi\theta^2)^3}{N^3} \sum_{i,j,k=1}^N Q_i Q_j Q_k \epsilon_{ti} \epsilon_{tj} \epsilon_{tk} . \quad (5.32)$$

It is easy to show, using the methods used before, that  $E(M_3) = \langle M_{\text{ap}}^3 \rangle$ . An estimator for an ensemble of fields can then be defined immediately in analogy to (5.19).

## 6 Discussion and conclusions

In this paper we have introduced the  $M_{\text{ap}}$ -statistics, or mass-aperture statistics, as a new measure for cosmic shear. We have compared those statistics with others suggested earlier, namely the shear two-point correlation function, and the rms of the shear averaged over circles. The main results can be summarized as follows:

(1)  $M_{\text{ap}}$  is defined as a filtered version of the projected density field  $\kappa$ , but can be calculated in terms of the tangential shear inside a circular aperture. Hence,  $M_{\text{ap}}$  has a well-defined physical interpretation, and at the same time can be expressed in terms of the observable shear.

(2) The dispersion of  $M_{\text{ap}}$ ,  $\langle M_{\text{ap}}^2(\theta) \rangle$ , can be expressed as a convolution of the power spectrum of the projected density field with a filter function which is strongly peaked. In contrast, the corresponding filter function for the rms of the shear averaged over circles is considerably broader and in particular picks up the long wavelength range of the power spectrum. Therefore, the  $M_{\text{ap}}$ -statistics has the nice property of being a well localized measure for the projected density field. From measurements on different angular scales, the power spectrum of the projected density field can be constructed. A different method to obtain a local estimate of the power spectrum of the projected density field has recently been suggested by Kaiser (1996).

(3) In contrast to the mean shear inside a circle,  $M_{\text{ap}}$  is a scalar quantity. It is therefore possible to define the skewness of  $M_{\text{ap}}$  which is measurable.

(4) Whereas  $\langle M_{\text{ap}}^2(\theta) \rangle$  is smaller than  $\langle |\bar{\gamma}(\theta)|^2 \rangle$ , at least on small scales, the dispersion of the estimator for  $\langle M_{\text{ap}}^2 \rangle$  is smaller by a factor of  $\sqrt{2}$  than that for  $\langle |\bar{\gamma}(\theta)|^2 \rangle$  on small scales, due to the fact that in the former case, only one component of the shear is needed for the estimate. On scales beyond a few arcminutes, the dispersion of the estimates for both statistics is dominated by the cosmic variance, so that the fractional accuracy of the estimates is nearly  $N_f^{-1/2}$ , where  $N_f$  is the number of independent circular apertures.

(5) The values of  $M_{\text{ap}}$  for neighboring circles decorrelates very rapidly with increasing separation. In particular, we found that the values of  $M_{\text{ap}}$  calculated on circles which just touch are nearly mutually independent, with a correlation coefficient below  $10^{-2}$ . This implies that one can make use of wide-field images by ‘punching’ circles on these images and considering the  $M_{\text{ap}}$  values on these circles as mutually independent. In contrast to that, the mean shear inside neighboring circles is very strongly correlated, and these have to be separated by several degrees before they can be considered independent. Therefore, the  $M_{\text{ap}}$ -statistics provides a very valuable tool for measuring cosmic shear on scales of arcminutes from wide-field images. A single one square degree image of sufficient depth (e.g., corresponding to a few hours integration time on a 4-meter-class telescope) and high imaging quality can be used to obtain  $\langle M_{\text{ap}}^2(\theta) \rangle$  on scales below  $\sim 5'$  with a signal-to-noise larger than  $\sim 3$ . The signal-to-noise is proportional to the square root of the solid angle covered by the available data.

(6) The skewness of  $M_{\text{ap}}$  is very sensitive to the cosmological model, but rather independent of the shape of the power spectrum. In particular, in the quasilinear regime, the skewness is independent of the normalization of the power spectrum. Whereas the latter property may not be strictly preserved when considering the skewness in a fully non-linearly evolved density field, the experience from comparing numerical simulations of the density field with quasi-linear predictions has shown that at least the skewness of the density field is rather well approximated by quasi-linear theory, even for density contrasts of order unity (Baugh et al 1995, Colombi et al. 1996, Gaztañaga & Bernardeau 1997). We therefore expect that the independence of the skewness on the normalization will be roughly preserved in the non-linear case. This makes the skewness a very valuable probe for cosmological parameters.

(7) The difference between the predictions from linear evolution of the cosmic density fluctuations, and the fully non-linear evolution of the power spectrum, is much larger for the  $m$ -statistics than for the mean shear within circles – see Fig. 3. This is related to the fact that the filter function for  $\langle M_{\text{ap}}^2 \rangle$  is narrowly peaked, whereas the corresponding filter for  $\langle |\bar{\gamma}(\theta)|^2 \rangle$  has a long tail towards long wavelengths. Since the long wavelengths have not become non-linear (see Fig. 1), the non-linear effects for  $\langle |\bar{\gamma}(\theta)|^2 \rangle$  are necessarily weaker than for  $\langle M_{\text{ap}}^2 \rangle$ .

The signal-to-noise estimates given in this paper suffer from the lack of knowledge on the kurtosis of  $M_{\text{ap}}$ , which we have not attempted to calculate, or more generally, the distribution function of  $M_{\text{ap}}$ . Therefore, the estimate presented in Fig. 7 may be slightly optimistic. A more accurate estimate can be obtained from numerical simulations, by taking high-resolution realizations of the cosmic mass distribution and studying light propagation through such a Universe. Such studies have been undertaken in various ways

and with various scientific goals in the past (e.g., Jaroszyński et al. 1990, Lee & Paczyński 1990, Bartelmann & Schneider 1991, Jaroszyński 1991, 1992, Wambsganss et al. 1995, 1997). In particular, Blandford et al. (1991) have compared their analytical estimates for the rms shear inside circles with results from numerical ray propagation simulations. Further work in this direction will most useful. In particular, the performance of practical estimators for the dispersions and skewness can be evaluated, and the accuracy of the approximations used here (i.e., the Born approximation and the neglect of lens-lens terms in (2.10)) can be checked.

In summary, the  $M_{\text{ap}}$ -statistics appears to be an attractive measure for cosmic shear. We expect that its applications can be expanded beyond the range considered here. It is a promising method to search for mass concentrations in the Universe, as pointed out in Schneider (1996). A further application may include the correlation of shear, as measured by  $M_{\text{ap}}$ , with the distribution of foreground galaxies, measured through the same filter function  $U$ . We shall exploit this route as a method for measuring the bias parameter, and its dependence on scale, in a later publication.

We are grateful to many colleagues for discussions on the topic of this paper; in particular, we want to thank M. Bartelmann, F. Bernardeau, S. Mao, Y. Mellier, S. Seitz and S. White for many helpful suggestions and discussions, and M. Bartelmann and S. White for a careful reading of the manuscript. This work was supported by the ‘‘Sonderforschungsbereich 375-95 für Astro-Teilchenphysik’’ der Deutschen Forschungsgemeinschaft, by the Programme National de Cosmologie of the Centre National de la Recherche Scientifique in France, and by EU contract CHRX CT930120.

## Appendix

In this Appendix we calculate the contributions to the (observable) skewness which would be present even in the case of a Gaussian density field. The three effects which cause a non-zero value for  $\langle M_{\text{ap}}^3 \rangle$  also for Gaussian fields are: (1) Image ellipticities provide an unbiased estimate of the reduced shear  $g = \gamma/(1 - \kappa)$ , rather than the shear  $\gamma$  itself. (2) The separation vector  $\mathbf{x}(\boldsymbol{\theta}, w)$  deviates from  $f_K(w)\boldsymbol{\theta}$  – see (2.7); the (‘Born’) approximation leading from (2.9) to (2.10) neglects this effect. (3) Also, in the same step, the matrix  $\mathcal{A}$  on the right-hand-side of (2.9) was approximated by the unit matrix; therefore, (2.10) does not contain the coupling between deflectors at different redshifts. The two latter terms have already been discussed, in somewhat different context, in BvWM. We shall consider here these effects in turn. In this Appendix,  $\delta$  and  $\Phi$  are meant to be the *linear* density field and its corresponding gravitational potential, since we are interested in the contribution to the skewness coming from the above-mentioned effects in the presence of a Gaussian field.

### A1 Aperture mass in terms of $g$

Let

$$g_t(\boldsymbol{\vartheta}) = \frac{\gamma_t(\boldsymbol{\vartheta})}{1 - \kappa(\boldsymbol{\vartheta})} \quad (\text{A1})$$

be the tangential component of the reduced shear. Then, from image ellipticities, one obtains an unbiased estimate of

$$M_g(\theta) := \int d^2\vartheta Q(|\vartheta|) g_t(\vartheta) = M_{\text{ap}}(\theta) + \delta M_{\text{ap}}(\theta), \quad (\text{A2})$$

where

$$\delta M_{\text{ap}}(\theta) \approx \int d^2\vartheta Q(|\vartheta|) \kappa(\vartheta) \gamma_t(\vartheta). \quad (\text{A3})$$

Hence, the observable skewness becomes

$$\langle M_g^3(\theta) \rangle \approx \langle M_{\text{ap}}^3(\theta) \rangle + 3 \langle M_{\text{ap}}^2(\theta) \delta M_{\text{ap}}(\theta) \rangle \equiv \langle M_{\text{ap}}^3(\theta) \rangle + \delta \langle M_{\text{ap}}^3(\theta) \rangle_g. \quad (\text{A4})$$

Using the fact that the Fourier transform of the shear is  $\tilde{\gamma}(\mathbf{s}) = \tilde{\kappa}(\mathbf{s}) e^{2i\varphi_s}$ , where  $\varphi_s$  is the polar angle of  $\mathbf{s}$ , the tangential shear – see (3.9) – can be Fourier-decomposed as

$$\gamma_t(\vartheta) = -\mathcal{R}e \left( \int \frac{d^2s}{(2\pi)^2} e^{2i\varphi_s} \tilde{\kappa}(\mathbf{s}) e^{i\mathbf{s}\cdot\vartheta} e^{-2i\varphi} \right) = - \int \frac{d^2s}{(2\pi)^2} \cos 2(\varphi - \varphi_s) e^{i\mathbf{s}\cdot\vartheta} \tilde{\kappa}(\mathbf{s}), \quad (\text{A5})$$

where in the last step use was made of the fact that  $\kappa(\vartheta)$  is real, and  $\varphi$  is the polar angle of  $\vartheta$ . Then, from the definition in (A4) and by introducing the expression (3.5) for  $M_{\text{ap}}(\theta)$ , one obtains after replacing  $\kappa(\vartheta)$  by its Fourier representation:

$$\begin{aligned} \delta \langle M_{\text{ap}}^3(\theta) \rangle_g &= -3 \int d^2\vartheta_1 U(|\vartheta_1|) \int \frac{d^2s_1}{(2\pi)^2} e^{i\mathbf{s}_1\cdot\vartheta_1} \int d^2\vartheta_2 U(|\vartheta_2|) \int \frac{d^2s_2}{(2\pi)^2} e^{i\mathbf{s}_2\cdot\vartheta_2} \\ &\times \int d^2\vartheta Q(|\vartheta|) \int \frac{d^2s'}{(2\pi)^2} e^{i\mathbf{s}'\cdot\vartheta} \int \frac{d^2s}{(2\pi)^2} \cos 2(\varphi - \varphi_s) e^{i\mathbf{s}\cdot\vartheta} \langle \tilde{\kappa}(\mathbf{s}_1) \tilde{\kappa}(\mathbf{s}_2) \tilde{\kappa}(\mathbf{s}) \tilde{\kappa}(\mathbf{s}') \rangle. \end{aligned} \quad (\text{A6})$$

We calculate the correction  $\delta \langle M_{\text{ap}}^3 \rangle_g$  to leading order and thus use the linear evolution of the cosmic density fluctuations. In this approximation the density field remains Gaussian, and since  $\kappa$  is a linear functional of the density fluctuations,  $\kappa$  is Gaussian. Then the correlator in (A6) becomes

$$\begin{aligned} \langle \tilde{\kappa}(\mathbf{s}_1) \tilde{\kappa}(\mathbf{s}_2) \tilde{\kappa}(\mathbf{s}) \tilde{\kappa}(\mathbf{s}') \rangle &= (2\pi)^4 P_\kappa(s_1) P_\kappa(s') \delta_{\text{D}}(\mathbf{s}_1 + \mathbf{s}_2) \delta_{\text{D}}(\mathbf{s}' + \mathbf{s}) \\ &+ 2 \text{ terms obtained from permutation.} \end{aligned} \quad (\text{A7})$$

Inserting (A7) into (A6), one notices that the first term yields zero, whereas the other two terms yield equal contributions. After carrying out the  $\mathbf{s}_1$  and  $\mathbf{s}_2$  integrations, one finds

$$\begin{aligned} \delta \langle M_{\text{ap}}^3(\theta) \rangle_g &= -6 \int d^2\vartheta_1 U(|\vartheta_1|) \int d^2\vartheta_2 U(|\vartheta_2|) \int d^2\vartheta Q(|\vartheta|) \\ &\times \int \frac{d^2s}{(2\pi)^2} \cos 2(\varphi - \varphi_s) e^{i\mathbf{s}\cdot(\vartheta - \vartheta_1)} P_\kappa(s) \int \frac{d^2s'}{(2\pi)^2} e^{i\mathbf{s}'\cdot(\vartheta - \vartheta_2)} P_\kappa(s'). \end{aligned} \quad (\text{A8})$$

Next, we perform the polar angle integration of  $\vartheta_1$  and  $\vartheta_2$ , and use the definition of the filter  $I_\ell(\eta)$  to obtain

$$\begin{aligned} \delta \langle M_{\text{ap}}^3(\theta) \rangle_g &= -6 \int d^2\vartheta Q(|\vartheta|) \int \frac{d^2s}{(2\pi)^2} \cos 2(\varphi - \varphi_s) e^{i\mathbf{s}\cdot\vartheta} P_\kappa(s) I_\ell(s\theta) \\ &\times \int d^2s' e^{i\mathbf{s}'\cdot\vartheta} P_\kappa(s') I_\ell(s'\theta). \end{aligned} \quad (\text{A9})$$

Finally, the three integrations over the polar angles can be carried out, leaving the final result

$$\begin{aligned} \delta \langle M_{\text{ap}}^3(\theta) \rangle_g &= 12\pi \int ds s P_\kappa(s) I_\ell(s\theta) \int ds' s' P_\kappa(s') I_\ell(s'\theta) \\ &\times \int_0^\theta d\vartheta \vartheta Q(\vartheta) J_0(\vartheta s') J_2(\vartheta s). \end{aligned} \quad (\text{A10})$$

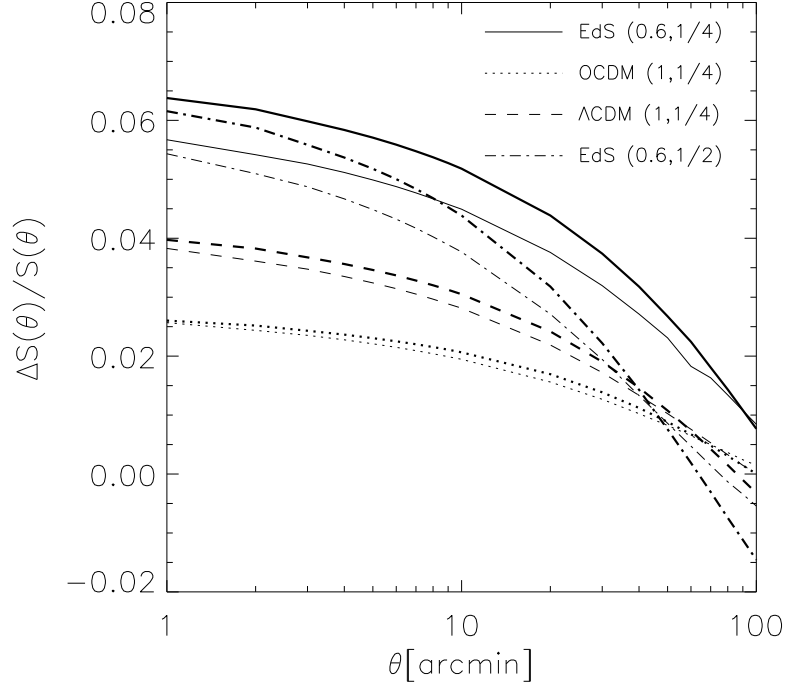


**Fig. 9.** The fractional change of the skewness which occurs by considering  $\langle M_{\text{ap}}^3 \rangle$  instead of  $\langle M_g^3 \rangle$ , where the latter one is the observable quantity, for four different cosmological models (thick curves). For comparison, the thin curves show the corrections due to the Born approximation and the neglect of lens-lens coupling terms in (2.10). In this figure, the sources were assumed to follow the redshift distribution (2.18), with  $z_0 = 1$  and  $\beta = 1.5$

In Fig. 9 we have plotted the fractional contribution  $\delta \langle M_{\text{ap}}^3(\theta) \rangle_g / \langle M_{\text{ap}}^3(\theta) \rangle$  as a function of angular scale  $\theta$ , for four different cosmological models. As can be seen, the difference between  $\langle M_g^3 \rangle$  and  $\langle M_{\text{ap}}^3 \rangle$  is very small, lower than 6% for all cases considered, where the largest deviations occur in the EdS models.

## A2 Lens-lens coupling, and dropping the Born approximation

The expression (2.10) for the Jacobi matrix  $\mathcal{A}$  is valid up to first order in the gravitational potential  $\Phi$ . The two effects considered here are obtained by expanding (2.9) up to second order in  $\Phi$ .

We write (2.7) as  $\mathbf{x}(\boldsymbol{\theta}, w) = \mathbf{x}^{(0)}(\boldsymbol{\theta}, w) + \mathbf{x}^{(1)}(\boldsymbol{\theta}, w) + \mathcal{O}(\Phi^2)$ , with  $\mathbf{x}^{(0)}(\boldsymbol{\theta}, w) = f_K(w)\boldsymbol{\theta}$  and  $\mathbf{x}^{(1)}(\boldsymbol{\theta}, w)$  given by the second term in (2.7), now with  $\mathbf{x}$  in the integrand replaced by  $\mathbf{x}^{(0)}$ . Similarly, we write  $\mathcal{A}(\boldsymbol{\theta}, w) = \mathcal{A}^{(0)}(\boldsymbol{\theta}, w) + \mathcal{A}^{(1)}(\boldsymbol{\theta}, w) + \mathcal{A}^{(2)}(\boldsymbol{\theta}, w) + \mathcal{O}(\Phi^3)$ , with  $\mathcal{A}_{ij}^{(0)}(\boldsymbol{\theta}, w) = \delta_{ij}$ , and  $\mathcal{A}^{(1)}(\boldsymbol{\theta}, w)$  given by the second term of (2.10). Expanding (2.9) in terms of  $\Phi$ , one finds that

$$\begin{aligned} \mathcal{A}_{ij}^{(2)}(\boldsymbol{\theta}, w) &= -\frac{2}{c^2} \int_0^w dw' \frac{f_K(w-w')f_K(w')}{f_K(w)} \\ &\times \left[ \Phi_{,ikl}(f_K(w')\boldsymbol{\theta}, w') x_l^{(1)}(\boldsymbol{\theta}, w') \delta_{kj} + \Phi_{,ik}(f_K(w')\boldsymbol{\theta}, w') \mathcal{A}_{kl}^{(1)}(\boldsymbol{\theta}, w') \right], \end{aligned} \quad (\text{A11})$$

which, after inserting the expressions for  $\mathbf{x}^{(1)}$  and  $\mathcal{A}^{(1)}$  yields

$$\begin{aligned} \mathcal{A}_{ij}^{(2)}(\boldsymbol{\theta}, w) &= \frac{4}{c^4} \int_0^w dw' \frac{f_K(w-w')f_K(w')}{f_K(w)} \int_0^{w'} dw'' f_K(w'-w'') \\ &\times \left[ \Phi_{,ijl}(f_K(w')\boldsymbol{\theta}, w') \Phi_{,l}(f_K(w'')\boldsymbol{\theta}, w'') \right. \\ &\left. + \frac{f_K(w'')}{f_K(w')} \Phi_{,ik}(f_K(w')\boldsymbol{\theta}, w') \Phi_{,kj}(f_K(w'')\boldsymbol{\theta}, w'') \right]. \end{aligned} \quad (\text{A12})$$

We consider 1/2 of the trace of  $\mathcal{A}^{(2)}$  as the surface mass density to second order in  $\Phi$ . Although  $\mathcal{A}^{(2)}$  is in general not symmetric, so that to this order the lens mapping can no longer be described by an equivalent surface mass density, the asymmetry is expected to be small in realistic situations, and we shall neglect it henceforth. Then, after averaging over a source redshift distribution, as done in (2.15), and replacing the derivatives of  $\Phi$  by their Fourier representation, using the Poisson equation (2.13), one finds

$$\begin{aligned} \kappa^{(2)}(\boldsymbol{\theta}) &= \frac{9}{2} \left( \frac{H_0}{c} \right)^4 \Omega_d^2 \int_0^{w_H} dw' g(w') \frac{f_K(w')}{a(w')} \int_0^{w'} dw'' \frac{f_K(w'-w'')}{a(w'')} \\ &\times \int \frac{d^3 k'}{(2\pi)^3} \frac{1}{|\vec{k}'|^2} \exp [i (k'_3 w' + f_K(w') \mathbf{k}' \cdot \boldsymbol{\theta})] \tilde{\delta}(\vec{k}'; w') \\ &\times \int \frac{d^3 k''}{(2\pi)^3} \frac{1}{|\vec{k}''|^2} \exp [i (k''_3 w'' + f_K(w'') \mathbf{k}'' \cdot \boldsymbol{\theta})] \tilde{\delta}(\vec{k}''; w'') \\ &\times \left[ \frac{f_K(w'')}{f_K(w')} (\mathbf{k}' \cdot \mathbf{k}'')^2 + |\mathbf{k}'|^2 \mathbf{k}' \cdot \mathbf{k}'' \right], \end{aligned} \quad (\text{A13})$$

where we use the same notation as in the main text, i.e.,  $\vec{k}$  has  $\mathbf{k}$  as the first two components.

To calculate the resulting contribution to the skewness according to (4.1), we note that

$$\langle \kappa(\boldsymbol{\theta}_1) \kappa(\boldsymbol{\theta}_2) \kappa(\boldsymbol{\theta}_3) \rangle \doteq 3 \left\langle \kappa^{(1)}(\boldsymbol{\theta}_1) \kappa^{(1)}(\boldsymbol{\theta}_2) \kappa^{(2)}(\boldsymbol{\theta}_3) \right\rangle + \mathcal{O}(\Phi^5), \quad (\text{A14})$$

where the ‘ $\doteq$ ’-sign means that the two expressions yield the same result after insertion into (4.1), owing to the symmetry of the integration there. The correlator in (A14) is calculated by inserting (A13) for  $\kappa^{(2)}$ , and (2.15), with  $\delta$  replaced by its Fourier decomposition, for  $\kappa^{(1)}$ . The resulting expression then contains a correlation function of four  $\tilde{\delta}$ -terms. Since we consider the lowest, i.e., the linear order of  $\delta$ , the four-point correlation function is given by (4.9). Using arguments very similar to those which led from (4.3) to (4.5), one finds



$$\begin{aligned}
3 \langle \kappa^{(1)}(\boldsymbol{\theta}_1) \kappa^{(1)}(\boldsymbol{\theta}_2) \kappa^{(2)}(\boldsymbol{\theta}_3) \rangle &= \frac{243}{4} \left( \frac{H_0}{c} \right)^8 \Omega_d^4 \int_0^{w_H} dw \left( \frac{g(w) f_K(w) D_+(w)}{a(w)} \right)^2 \\
&\times \int_0^w dw' \frac{g(w') f_K(w') f_K(w-w') D_+^2(w')}{a^2(w')} \int \frac{d^2 k}{(2\pi)^2} P_0(k) \exp(i f_K(w) \mathbf{k} \cdot (\boldsymbol{\theta}_1 - \boldsymbol{\theta}_3)) \\
&\times \int \frac{d^2 k'}{(2\pi)^2} P_0(k') \exp(i f_K(w') \mathbf{k}' \cdot (\boldsymbol{\theta}_2 - \boldsymbol{\theta}_3)) \left[ \frac{f_K(w')}{f_K(w)} \frac{(\mathbf{k} \cdot \mathbf{k}')^2}{|\mathbf{k}|^2 |\mathbf{k}'|^2} + \frac{\mathbf{k} \cdot \mathbf{k}'}{|\mathbf{k}'|^2} \right].
\end{aligned} \tag{A15}$$

As a final step, we change variables to  $\mathbf{s} = f_K(w) \mathbf{k}$ ,  $\mathbf{s}' = f_K(w') \mathbf{k}'$ , and insert the resulting expression into (4.1), using (A14). After applying the definition of  $I_\ell$ , the contribution to the skewness from lens-lens coupling and dropping the Born approximation becomes

$$\begin{aligned}
\delta \langle M_{\text{ap}}^3(\theta) \rangle_{\text{B+C}} &= \frac{243}{8\pi} \left( \frac{H_0}{c} \right)^8 \Omega_d^4 \int_0^{w_H} dw \left( \frac{g(w) D_+(w)}{a(w)} \right)^2 \\
&\times \int_0^w dw' \frac{g(w') f_K(w-w') D_+^2(w')}{a^2(w') f_K(w)} \\
&\times \int d^2 s P_0 \left( \frac{s}{f_K(w)} \right) \int d^2 s' P_0 \left( \frac{s'}{f_K(w')} \right) \\
&\times \left[ \frac{(\mathbf{s} \cdot \mathbf{s}')^2}{|\mathbf{s}|^2 |\mathbf{s}'|^2} + \frac{\mathbf{s} \cdot \mathbf{s}'}{|\mathbf{s}'|^2} \right] I_\ell(\theta s) I_\ell(\theta s') I_\ell(\theta |\mathbf{s} + \mathbf{s}'|).
\end{aligned} \tag{A16}$$

We have plotted this correction term, together with  $\delta \langle M_{\text{ap}}^3 \rangle_g$ , in Fig. 9. There we can see that this correction term is of the same order as that considered in the previous subsection, i.e., smaller than  $\sim 5\%$  on scales larger than 1 arcmin. These corrections are therefore smaller than the uncertainties introduced by calculating the skewness with quasi-linear theory. A numerical ray-trace calculation would of course take all the correction effects mentioned here into account.

It turns out that  $\Delta S$  is nearly independent of cosmology; this can be traced back to the fact that  $\delta \langle M_{\text{ap}}^3 \rangle$  and  $\langle M_{\text{ap}}^2 \rangle^2$  can be expressed as bilinear functions of the projected power spectrum  $P_\kappa$ . Assume for a moment that locally,  $P_\kappa(s)$  is a power law; then  $\Delta S$  would depend only on the local slope of this power law, independent of cosmological factors. Hence, if the local slopes of the power spectra in different cosmological models are similar, one expects  $\Delta S$  to be nearly independent of the cosmological model.

## References

- Bartelmann, M. & Schneider, P. 1991, A&A 248, 349  
Bartelmann, M. & Schneider, P. 1994, A&A 284, 1.  
Baugh, C., Gaztañaga, E. & Efstathiou, G. 1995, MNRAS 274, 1049  
Benítez, N. & Martínez-González, E. 1997, ApJ 477, 27  
Bernardeau, F., van Waerbeke, L. & Mellier, Y. 1997, A&A 322, 1 (BvWM)  
Blandford, R.D. & Jaroszyński, M. 1981, ApJ 246, 1  
Blandford, R.D., Saust, A.B., Brainerd, T.G. & Villumsen, J.V. 1991, MNRAS 251, 600  
Bonnet, H. & Mellier, Y. 1995, A&A 303, 331.

- Bouchet, F., Juszkiewicz, R., Colombi, S. & Pellat, R. 1992, ApJ 394, L5.
- Bower, R. & Smail, I. 1997, astro-ph/9612151
- Colombi, S., Bouchet F.R. & Hernquist L. 1996, ApJ, 465, 14
- Efstathiou, G. 1996, in: *Cosmology and large scale structure*, Les Houches Session LX, R. Schaeffer, J. Silk, M. Spiro & J. Zinn-Justin (eds.), North-Holland, p. 133.
- Fahlman, G., Kaiser, N., Squires, G. & Woods, D. 1994, ApJ 437, 56.
- Fort, B., Mellier, Y., Dantel-Fort, M., Bonnet, H. & Kneib, J.-P. 1996, A&A 310, 705
- Fry, J.N. 1984, ApJ 279, 499.
- Gaztañaga, E. & Bernardeau, F. 1997, astro-ph/9707095
- Goroff, M.H., Grinstein, B., Rey, S.J. & Wise, M.B. 1986, MNRAS 236, 385.
- Gunn, J.E. 1967, ApJ 147, 61
- Hamilton, A.J.S., Kumar, P., Lu, E. & Matthews, A. 1991, ApJ 374, L1
- Jain, B., Mo, H. & White, S.D.M. 1995, MNRAS 276, L25
- Jain, B. & Seljak, U. 1997, ApJ, in press (JS)
- Jaroszyński, M. 1991, MNRAS 249, 430
- Jaroszyński, M. 1992, MNRAS 255, 655
- Jaroszyński, M., Park, C., Paczyński, B. & Gott, J.R. 1990, ApJ 365, 22
- Kaiser, N. 1992, ApJ 388, 272
- Kaiser, N. 1995, ApJ 439, L1
- Kaiser, N. 1996, astro-ph/9610120 (K96)
- Kaiser, N., Squires, G. & Broadhurst, T. 1995, ApJ 449, 460.
- Kaiser, N., Squires, G., Fahlman, G. & Woods, D. 1994, in: *Clusters of Galaxies*, eds. F. Durret, A. Mazure & J. Tran Thanh Van, Editions Frontieres.
- Lee, M.H. & Paczyński, B. 1990, ApJ 357, 32
- Luppino, G. & Kaiser, N. 1997, ApJ 475, 20.
- Mould, J. et al. 1994, MNRAS 271, 31.
- Peacock, J.A. & Dodds, S.J. 1996, MNRAS 280, L19
- Schneider, P. 1996, MNRAS 283, 837
- Schneider, P., van Waerbeke, L., Mellier, Y., Jain, B., Seitz, S. & Fort, B. 1997, astro-ph/9705122
- Seitz, S., Schneider, P. & Ehlers, J. 1994, Class. Quant. Grav. 11, 2345
- Smail, I., Hogg, D.W., Yan, L. & Cohen, J.G. 1995, ApJ, 449, L105
- van Waerbeke, L., Mellier, Y., Schneider, P., Fort, B. & Mathez, G. 1997, A&A, 317, 303.
- Villumsen, J. 1995, astro-ph/9507007
- Villumsen, J. 1996, MNRAS 281, 369.
- Wambsganss, J., Cen, R., Ostriker, J.P. & Turner, E.L. 1995, Science 268, 274
- Wambsganss, J., Cen, R., Xu, G. & Ostriker, J.P. 1997, ApJ 475, L81